

# Finite-Difference Schemes for Anisotropic Diffusion

Bram van Es <sup>\*†</sup>, Barry Koren <sup>‡</sup> and Hugo J. de Blank <sup>†</sup>

## Abstract

In fusion plasmas diffusion tensors are extremely anisotropic due to the high temperature and large magnetic field strength. This causes diffusion, heat conduction, and viscous momentum loss, to effectively be aligned with the magnetic field lines. This alignment leads to different values for the respective diffusive coefficients in the magnetic field direction and in the perpendicular direction, to the extent that heat diffusion coefficients can be up to  $10^{12}$  times larger in the parallel direction than in the perpendicular direction. This anisotropy puts stringent requirements on the numerical methods used to approximate the MHD-equations since any misalignment of the grid may cause the perpendicular diffusion to be polluted by the numerical error in approximating the parallel diffusion. Currently the common approach is to apply magnetic field-aligned coordinates, an approach that automatically takes care of the directionality of the diffusive coefficients. This approach runs into problems at x-points and at points where there is magnetic re-connection, since this causes local non-alignment. It is therefore useful to consider numerical schemes that are tolerant to the misalignment of the grid with the magnetic field lines, both to improve existing methods and to help open the possibility of applying regular non-aligned grids. To investigate this, in this paper several discretisation schemes are developed and applied to the anisotropic heat diffusion equation on a non-aligned grid.

Keywords: anisotropic diffusion, finite differences

## 1 Introduction

Anisotropic diffusion is a common physical phenomenon and describes processes where the diffusion of some scalar quantity is direction dependent. Anisotropic diffusive processes are for instance transport in porous media, large-scale turbulence where turbulence scales are anisotropic in size, and of interest to us: heat conduction and momentum dissipation in fusion plasmas.

In tokamak fusion plasmas the viscosity and heat conduction coefficient parallel to the magnetic field may be in the order of  $10^6$  and  $10^{12}$  times larger, respectively, than perpendicular conduction coefficients. This is caused by the fact that the heat conductivity parallel and perpendicular to the magnetic field lines are determined by different physical processes; along the field lines particles can travel relatively large distances without collision whereas perpendicular to the field lines the mean free path is in the order of the gyroradius, see e.g. Hölzl [37].

Numerically, high anisotropy may lead to the situation that errors in the direction of the largest diffusion coefficient may significantly influence the diffusion in the perpendicular direction. This necessitates a high-order approximation in the direction of the largest coefficient value (see e.g. Sovinec et al. [65], Meier et al. [54]). Given the high level of anisotropy in tokamak plasmas, a numerical approximation may introduce large perpendicular errors if the magnetic field direction is strongly misaligned with the grid. Problems that may arise with highly anisotropic diffusion problems on non-aligned meshes are in general:

---

<sup>\*</sup>Centrum Wiskunde & Informatica, es@cwi.nl, P.O. Box 94079, 1090GB Amsterdam, the Netherlands

<sup>†</sup>FOM Institute DIFFER, Dutch Institute for Fundamental Energy Research, Association EURATOM-FOM, the Netherlands, www.differ.nl

<sup>‡</sup>Eindhoven University of Technology, the Netherlands

- significant numerical diffusion perpendicular to the magnetic field lines due to grid misalignment, see e.g. Umansky et al. [66],
- non-positivity near high gradients, see e.g. Sharma et al. [63],
- mesh locking, stagnation of convergence dependent on anisotropy, see e.g. Babuška and Suri [9],
- convergence loss in case of variable diffusion tensor, see e.g. Günter et al. [31].

It is possible to use a field-aligned coordinate system. However this cannot be maintained throughout the plasma; problems arise at x-points and in regions of highly fluctuating magnetic field directions (for instance in case of edge turbulence). To confidently perform simulations of phenomena that rely heavily on the resolution of the perpendicular temperature gradient we must apply a scheme that maintains sufficient accuracy in case of varying anisotropy and misalignment.

The bulk of the present methods are designed with discontinuous diffusion tensors in mind, and often on general and distorted non-uniform grids. We give an (inexhaustive) overview of methods used today, for details the reader is referred to the specific papers.

We start with the Multi-Point Flux Approximation (MPFA), a cell-centered finite volume method commonly used for approximating anisotropic diffusion with discontinuous tensors on distorted meshes, see e.g. Aavatsmark et al. [3–6], and Edwards and Rogers [25]. The MPFA uses cell-centered unknowns and connects the volumes using shared subcells with a local low-order interpolation of the primary unknowns. The method is robust in terms of diffusion tensor discontinuity as it is locally conservative, but the resulting diffusion operator is often non-symmetric and formal accuracy can not be maintained for higher levels of anisotropy. The MPFA method comes in various flavors, depending on how the fluxes are approximated, for instance the original MPFA-O and MPFA-U methods by Aavatsmark et al [3, 4] and more recent by Aavatsmark et al. [2] and Agelas et al. [7] respectively, the symmetric MPFA-L and MPFA-G methods. Potier [43] devised a cell-centered finite-volume method where the gradients are solved on each vertex by imposing flux continuity conditions, similar to the MPFA approach. Eymard et al. [26] devised a cell-centered finite-volume scheme using a special discrete gradient operator. Downside is the use of a parameter dependent on the lowest eigenvalue of the diffusion tensor, a parameter which is not anisotropy-independent. Maire and Breil [12, 52] apply a MPFA-like finite-volume method with cell-centered unknowns and a local variational formulation to obtain the fluxes in their Cell-Centered Lagrangian Diffusion (CCLAD) approach, with the requirement that temperature and sub-face normal fluxes are continuous. Maire and Breil [53] also constructed a CCLAD method where the fluxes are constructed using finite differences. Jacq et al. [40] expanded the method to three dimensions.

Le Potier and Ong [45] and Ong [59] devised a cell-centered method which makes use of a dual grid. The dual grid unknowns are chosen to be linear combinations of cell unknowns. This so-called Finite Element Cell-Centered (FECC) method uses less unknowns per cell compared to other dual grid methods which apply both cell-centered unknowns and cell-face or vertex unknowns. Another difference is the use of a third grid which is a sub-grid of the dual grid. The formal convergence of the FECC method seems to be maintained for discontinuous diffusion tensors with large values for the anisotropy [45].

Shashkov and Steinberg [64] constructed the Support Operator Method (SOM), also known as Mimetic Finite Difference (MFD) methods. Hyman et al. [38, 39] and Brezzi et al. [13, 14] apply and categorize the MFD methods. The MFD methods are mimetic to the extent that they preserve the self-adjointness of the divergence and the flux operator. Key to the MFD methods is the use of a dual grid, where flux values and temperature values are placed on separate grid points, and the application of a variational formulation to find the flux values, such that the self-adjointness between the discrete divergence operator and the discrete gradient operator is guaranteed. Downside of the original MFD schemes is the use of non-local operators. Formal convergence is robust for high levels of anisotropy, grid non-uniformity and discontinuous diffusion

tensors. Further, the diffusion operator is symmetric positive definite. Günter et al. [31] apply the MFD method to fusion plasma relevant test cases and maintain the order of accuracy for non-aligned (regular, rectangular) meshes. Günter et al. [30] apply the support-operator approach from Hyman et al. [39] to a finite-element method. The method is adapted to have a local flux description by Morel et al. [56], which requires both cell-centered and face-centered unknowns. The MFD method is finally made local and cell-centered by Lipnikov et al. [50] and Lipnikov and Shashkov [48].

Hermeline [33, 34] uses a dual grid, solving the diffusion equation on each grid where the temperature and the diffusion tensor values are defined in the same nodes. This is termed the Discrete Duality Finite-Volume (DDFV) method. The DDFV method requires the solution of the diffusion equation on two meshes and as such requires more unknowns. The resulting matrices are positive definite. Formal convergence for highly anisotropic problems (with the ratio between parallel and perpendicular diffusion coefficient  $10^{12}$ ) is close to second order for higher resolutions but not anisotropy-independent for coarser grids, see Potier and Ong [45]. The FECC method bears resemblance to the DDFV method where the former uses a third subgrid and cell-centered unknowns.

Other methods involving the use of dual grids are the Hybrid Finite Volume method (HFV) and the Mixed Finite Volume (MFV) method, see Eymard et al [27] and Droniou and Eymard [23] respectively. Droniou et al. [24] formally proved the similarity of the MFD scheme, the HFV scheme and the MFV scheme. The MFD, MFV, HFV and the DDFV methods can be placed within the concept of Compatible Discrete Operators (CDO) where the mathematical operators are treated exactly and the constitutive relations are approximated. Recent examples are the mimetic spectral element method developed by Kreeft et al. [42], applied to approximate Darcy flow with arbitrary order by Rebelo et al. [62]. Another example of a CDO method applied to anisotropic diffusion, similar to the work by Kreeft et al. is given by Bonelle and Ern [11]. Another approach is developed by Hirani [35], Desbrun et al [1] and is called Discrete Exterior Calculus, it is applied to scalar Darcy flow by Hirani et al [36].

Discontinuous Galerkin (DG) methods for elliptic problems have been developed that treat the diffusion equation as a system of first order equations, see Cockburn and Shu [15], Oden et al [58], and Peraire and Persson [61]. Discontinuous Galerkin applied to the original diffusion equation is performed using an interior penalty function by Douglas et al. [21] and through a mixed formulation of the diffusion terms by Bassi and Rebay [10]. A recovery based DG method for diffusion was developed by Van Leer and Nomura [68] and Van Leer et al [67]. Gassner et al. [29] approximate the numerical fluxes by solving the generalized Riemann problem.

Pasdunkorale and Turner [60] devised a Control Volume Finite Element method (CVFEM), which maintains the local flux continuity at the control volume faces for extreme anisotropy. Here the cross diffusion fluxes are partly resolved implicitly using least squares. This is not demonstrated for a full diffusion tensor with extreme anisotropy. The Vandermonde matrices for the least squares solution are based on the grid geometry, with no guarantee for well-posedness.

MPFA, MFD, CVFEM and other methods are somehow related, through flux-continuity requirement and a weak continuity requirement of the temperature over the edges, see Klausen and Russell [41]. Reference results for a variety of test cases can be found in Herbin and Hubert [32] and Eymard et al. [28]. For a more detailed overview of finite-volume methods the reader is referred to the review paper by Droniou [22].

All the methods discussed above leave the analytic formulation untouched and focus on the numerical procedure. In Degond et al. [16–18] and Mentrelli and Negulescu [55], the diffusion equation itself is split in two parts, a limit problem for infinite anisotropy and the original singular perturbation problem. Degond et al. [17] also provide a means for continuous transition between the two problems. This splitting is done to prevent ill-posedness which arises for Neumann boundary conditions and periodic boundary conditions. The

two formulations are obtained by discriminating between a mean part and a fluctuating part of the singular perturbation problem. These Asymptotic Preserving (AP) schemes have difficulties preserving accuracy and stability in case of closed field lines. Narski and Ottaviani [57] introduce a penalty stabilization term in the weak formulation of the AP-scheme to conserve accuracy in case of closed field lines. The downsides of this approach are that the penalty stabilization has a tuning parameter, it requires an  $L$ -stable time integration scheme and it requires the solution of two systems instead of one. An important benefit of AP-schemes is that the condition number does not scale with the anisotropy, without the use of a preconditioner.

Del-Castillo and Chacón [19, 20] apply a Lagrangian Green’s function approach that does not require any algorithmic inversion and thus prevents issues with ill-conditioning. However, this method is limited to a constant value for the parallel diffusion coefficient. Also the field lines are assumed to be time-invariant and it assumes a particular scaling for the variation of the magnetic field line strength.

None of the schemes is monotonous without special treatment of the linear operator or the mesh. Sharma et al. [63] apply a flux limiter to enforce the monotonicity locally but this is only applicable to relatively small levels of anisotropy not relevant for fusion plasma and it increases the perpendicular numerical diffusion and lowers the global accuracy. Methods that rely on changing the mesh basically change the elements based on the local values of the anisotropic diffusion to enforce that the local mass-matrices are  $M$ -matrices, see for instance Li and Huang [46], Aricò and Tucciarelli [8]. These methods are limited to low anisotropy. Monotonicity preserving methods that maintain the accuracy have been devised. These methods put restraints on the diffusion tensor and often require a nonlinear approach, see for instance Potier et al. [44], Lipnikov et al. [47, 49, 51].

In the present work the focus is on applying a co-located finite-difference discretisation in the direction of the strongest diffusion by means of interpolation. This can be applied to the flux operator only or to the entire operator. In this paper we try to live up to the accuracy properties of Günter et al.’s symmetric scheme by applying an interpolation scheme based on the direction of diffusion while still using a Cartesian grid. Furthermore we introduce a test case with elliptic closed field lines and we interpret the large difference in accuracy. We do not put any requirement on the diffusion tensor other than that it is symmetric. As we treat the singularly perturbed diffusion problem the scheme is not asymptotic preserving. For comparison we apply the asymmetric and symmetric finite-difference schemes given in Günter et al. [31].

We look at the order of convergence and the perpendicular numerical diffusion for extremely high levels of anisotropy.

## 2 Diffusion equation

Anisotropic thermal diffusion is described by the following model

$$\mathbf{q} = -\mathbf{D} \cdot \nabla T, \quad \frac{\partial T}{\partial t} = -\nabla \cdot \mathbf{q} + f, \quad (1)$$

where  $T$  represents temperature,  $\mathbf{b}$  the unit vector of the magnetic field line,  $f$  some source term and  $\mathbf{D}$  the diffusion tensor. For a two-dimensional problem the diffusion tensor is given by

$$\begin{aligned} \text{unit direction vector: } \mathbf{b} &= (\cos \alpha, \sin \alpha)^T, \\ \mathbf{D} &= (D_{\parallel} - D_{\perp})\mathbf{b}\mathbf{b}^T + D_{\perp}\mathcal{I}, \\ \mathbf{D} &= \begin{pmatrix} D_{\parallel}b_1^2 + D_{\perp}b_2^2 & (D_{\parallel} - D_{\perp})b_1b_2 \\ (D_{\parallel} - D_{\perp})b_1b_2 & D_{\perp}b_1^2 + D_{\parallel}b_2^2 \end{pmatrix}, \end{aligned}$$

where  $D_{\parallel}$  and  $D_{\perp}$  represent the parallel and the perpendicular diffusion coefficient respectively. We define  $x, y$  as the non-aligned coordinate system and  $s, n$  as the aligned coordinate system, see figure 1. The

boundary conditions are of Dirichlet type unless mentioned otherwise, they are discussed per test case. The diffusion equation is approximated on a uniform Cartesian grid, with  $\Delta x = \Delta y = h$ .

We define the anisotropy as

$$\zeta = \frac{D_{\parallel}}{D_{\perp}}.$$

In tokamak fusion plasma simulations the diffusion coefficients are often taken temperature-dependent. The

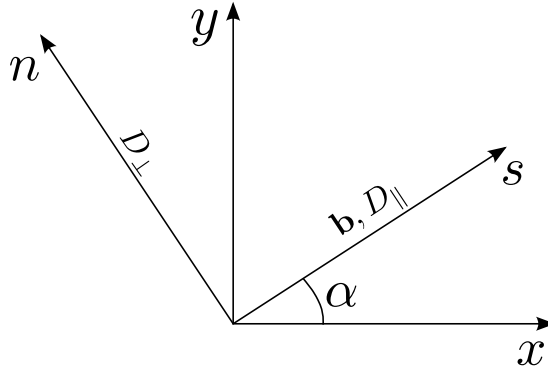


Figure 1: Explanation of symbols

parallel and perpendicular diffusion coefficient are assumed to be proportional to  $T^{5/2}$  and  $T^{-1/2}$  respectively. I.e. the anisotropy varies strongly with temperature. Note that the perpendicular diffusion coefficients are often assumed zero for fusion plasmas simulations, as the plasma is considered to be collisionless. For  $\zeta \rightarrow \infty$ , the problem reduces to

$$\frac{\partial T}{\partial t} = \nabla \cdot (D_{\parallel}(\mathbf{b} \cdot \nabla T)\mathbf{b}) = 0.$$

This limit problem has infinitely many solutions if  $\mathbf{b} \cdot \nabla T = 0$  and no temperature boundary conditions are prescribed for the field lines. So in the limit of the anisotropy going to infinity the diffusion equation may be ill-posed. This may occur when there are closed magnetic field lines. This is noticeable in the discretisation through a higher condition number of the linear operator for increasing anisotropy, see Degond et al. [16,17].

### 3 Finite-difference schemes

We limit the discussion to finite-difference schemes. Given a uniform grid this can be directly translated to a finite-volume approach. We consider several second-order accurate finite-difference schemes for the approximation of model equation (1). The first two schemes are described in Günter et al. [31]. The difference between these schemes lies in the treatment of the flux, particularly the location of the flux. The term co-located is used to indicate that the variables  $T$ ,  $\mathbf{b}$  are defined in coinciding points. The asymmetric and symmetric schemes, discussed in the following sections, have the field direction  $\mathbf{b}$  defined in the flux points and may be referred to as staggered schemes. The new schemes, to be presented here, aim to improve the accuracy of co-located schemes by applying a stencil that lies on an approximation of the field line. We use sub-indices  $x, y, s, n$  to denote the respective derivatives.

#### 3.1 Asymmetric finite differences

The first finite-difference scheme for heat diffusion we discuss is depicted in figure 2. For a spatially constant diffusion tensor this scheme reduces to the standard second-order accurate scheme for diffusion. The label

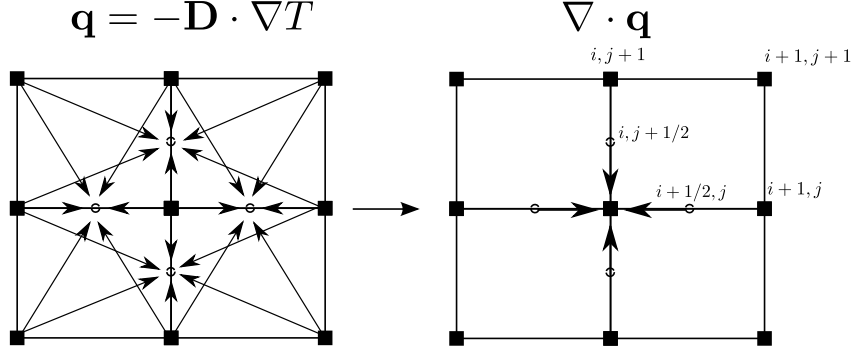


Figure 2: Asymmetric scheme, temperature  $T$  is defined on the full indices and the diffusion tensor  $\mathbf{D}$  on the half-indices

asymmetry is coined because of the different treatment of the  $x$ - and  $y$ -differential in each point. The different treatment is a direct result of taking the flux values in  $i \pm \frac{1}{2}, j$  and  $i, j \pm \frac{1}{2}$ ,

$$\begin{aligned} \left. \frac{\partial T}{\partial x} \right|_{i+\frac{1}{2},j} &= \frac{T_{i+1,j} - T_{i,j}}{\Delta x}, \\ \left. \frac{\partial T}{\partial y} \right|_{i+\frac{1}{2},j} &= \frac{T_{i+1,j+1} + T_{i,j+1} - T_{i,j-1} - T_{i+1,j-1}}{4\Delta y}, \\ \left. \frac{\partial T}{\partial x} \right|_{i,j+\frac{1}{2}} &= \frac{T_{i+1,j+1} + T_{i+1,j} - T_{i-1,j+1} - T_{i-1,j}}{4\Delta x}, \\ \left. \frac{\partial T}{\partial y} \right|_{i,j+\frac{1}{2}} &= \frac{T_{i,j+1} - T_{i,j}}{\Delta y}, \end{aligned}$$

and similar formulas for  $\left. \frac{\partial T}{\partial x} \right|_{i-\frac{1}{2},j}$ ,  $\left. \frac{\partial T}{\partial y} \right|_{i-\frac{1}{2},j}$ ,  $\left. \frac{\partial T}{\partial x} \right|_{i,j-\frac{1}{2}}$ ,  $\left. \frac{\partial T}{\partial y} \right|_{i,j-\frac{1}{2}}$ . For the heat conduction term we have

$$\mathbf{q}_{i+\frac{1}{2},j} = -\mathbf{D}_{i+\frac{1}{2},j} \cdot \left( \left. \frac{\partial T}{\partial x} \right|_{i+\frac{1}{2},j}, \left. \frac{\partial T}{\partial y} \right|_{i+\frac{1}{2},j} \right)^T.$$

Finally, the diffusion follows from

$$\nabla \cdot \mathbf{q} = \frac{(q_1)_{i+\frac{1}{2},j} - (q_1)_{i-\frac{1}{2},j}}{\Delta x} + \frac{(q_2)_{i,j+\frac{1}{2}} - (q_2)_{i,j-\frac{1}{2}}}{\Delta y}.$$

The scheme is denoted by *asymmetric scheme*, *G. et al.*

### 3.2 Symmetric finite differences

Still another approach is taken by Günter et al. [31]. They use a symmetric scheme (with a symmetric linear operator) that is mimetic by maintaining the self-adjointness of the differential operator. The approach goes

as follows. First, the divergence terms are determined at the center points, see figure 3:

$$\left. \frac{\partial T}{\partial x} \right|_{i+\frac{1}{2},j+\frac{1}{2}} = \frac{T_{i+1,j+1} + T_{i+1,j} - T_{i,j+1} - T_{i,j}}{2\Delta x},$$

$$\left. \frac{\partial T}{\partial y} \right|_{i+\frac{1}{2},j+\frac{1}{2}} = \frac{T_{i,j+1} + T_{i+1,j+1} - T_{i+1,j} - T_{i,j}}{2\Delta y}.$$

Next, the diffusion tensor is applied to obtain the heat flux

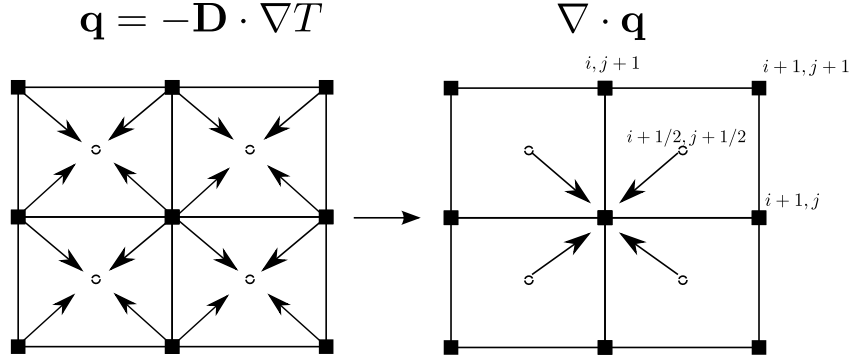


Figure 3: Symmetric scheme, temperature  $T$  is defined on the full indices and the diffusion tensor  $\mathbf{D}$  on the half-indices

$$\mathbf{q} = -\mathbf{D} \cdot \nabla T, \quad \mathbf{q}_{i+\frac{1}{2},j+\frac{1}{2}} = -\mathbf{D}_{i+\frac{1}{2},j+\frac{1}{2}} \cdot \left( \left. \frac{\partial T}{\partial x} \right|_{i+\frac{1}{2},j+\frac{1}{2}}, \left. \frac{\partial T}{\partial y} \right|_{i+\frac{1}{2},j+\frac{1}{2}} \right)^T.$$

Finally, the divergence is taken over the heat flux

$$\nabla \cdot \mathbf{q} = \frac{(q_1)_{i+\frac{1}{2},j+\frac{1}{2}} + (q_1)_{i+\frac{1}{2},j-\frac{1}{2}} - (q_1)_{i-\frac{1}{2},j+\frac{1}{2}} - (q_1)_{i-\frac{1}{2},j-\frac{1}{2}}}{2\Delta x} + \frac{(q_2)_{i+\frac{1}{2},j+\frac{1}{2}} + (q_2)_{i-\frac{1}{2},j+\frac{1}{2}} - (q_2)_{i-\frac{1}{2},j-\frac{1}{2}} - (q_2)_{i+\frac{1}{2},j-\frac{1}{2}}}{2\Delta y}.$$

The scheme is denoted by *symmetric scheme*, *G. et al.*

### 3.3 Treatment of fluxes

For the values of the diffusion coefficients  $D_{\parallel}, D_{\perp}$  in the flux points we have to apply averaging since they are dependent on the temperature which is known only in the surrounding points.

We use either arithmetic averaging or harmonic averaging. Harmonic averaging is relevant for plasma physics simulations if the density varies strongly. This may be the case if we consider turbulence at the edge for instance, see Sharma and Hammett [63]. For the asymmetric scheme by Günter et al we have, for flux point  $i + \frac{1}{2}, j$ :

$$\text{Arithmetic: } \mathbf{T}_{i+\frac{1}{2},j} = \frac{\mathbf{T}_{i+1,j} + \mathbf{T}_{i,j}}{2}, \quad \text{Harmonic: } \frac{2}{\mathbf{T}_{i+\frac{1}{2},j}} = \frac{1}{\mathbf{T}_{i+1,j}} + \frac{1}{\mathbf{T}_{i,j}}.$$

Analogous to the asymmetric scheme by Günter et al, for the symmetric scheme the diffusion tensor is either taken as the arithmetic mean or as the harmonic mean of the four surrounding points, e.g. for point  $i + \frac{1}{2}, j + \frac{1}{2}$ :

$$\begin{aligned} \text{Arithmetic: } \mathbf{T}_{i+\frac{1}{2},j+\frac{1}{2}} &= \frac{\mathbf{T}_{i+1,j+1} + \mathbf{T}_{i+1,j} + \mathbf{T}_{i,j+1} + \mathbf{T}_{i,j}}{4}, \\ \text{Harmonic: } \frac{4}{\mathbf{T}_{i+\frac{1}{2},j+\frac{1}{2}}} &= \frac{1}{\mathbf{T}_{i+1,j+1}} + \frac{1}{\mathbf{T}_{i+1,j}} + \frac{1}{\mathbf{T}_{i,j+1}} + \frac{1}{\mathbf{T}_{i,j}}. \end{aligned}$$

### 3.4 Aligned finite differences

The idea is that differencing along the field line yields an approximation less prone to large false perpendicular diffusion. To do this we have to use interpolation to find the values of  $T$  and  $\mathbf{D}$  on the field line. The field line trajectory itself is approximated by tracing. In the current implementation,  $T$ ,  $\mathbf{b}$  and  $\mathbf{D}$  are assumed to be coinciding. Using the definition for the diffusion tensor we can write the diffusion operator as

$$\nabla \cdot (\mathbf{D} \cdot \nabla T) = \nabla \cdot [(D_{\parallel} - D_{\perp}) \mathbf{b} \cdot \nabla T \mathbf{b}] + \nabla \cdot D_{\perp} \nabla T.$$

By now applying the product rule and some vector identities we can write the diffusion operator in parts:

$$\nabla \cdot (\mathbf{D} \cdot \nabla T) = \mathcal{A}_1 + \mathcal{A}_2 + \mathcal{A}_3 + \mathcal{A}_4, \quad (2)$$

where the parts are given by

$$\begin{aligned} \text{field line curvature: } \mathcal{A}_1 &= (D_{\parallel} - D_{\perp}) (\mathbf{b} \cdot \nabla \mathbf{b}) \cdot \nabla T, \\ \text{field strength gradient: } \mathcal{A}_2 &= (D_{\parallel} - D_{\perp}) (\nabla \cdot \mathbf{b}) (\mathbf{b} \cdot \nabla T), \\ \text{standard diffusion: } \mathcal{A}_3 &= (D_{\parallel} - D_{\perp}) \mathbf{b} \mathbf{b}^T : \nabla \nabla T + D_{\perp} \nabla^2 T, \\ \text{diffusion gradient: } \mathcal{A}_4 &= \mathbf{b} \cdot \nabla (D_{\parallel} - D_{\perp}) (\mathbf{b} \cdot \nabla T) + \nabla T \cdot \nabla D_{\perp}. \end{aligned}$$

The *field line curvature* term results from field line curvature in the presence of a temperature gradient and does not require a variation in the strength of the magnetic field. The *field strength variation* comes from the fact that we impose the constraint  $\nabla \cdot \mathbf{B} = 0$  on the MHD-equations so that

$$|\mathbf{B}| \nabla \cdot \mathbf{b} = -\mathbf{b} \cdot \nabla |\mathbf{B}|,$$

and thus  $\nabla \cdot \mathbf{b} \neq 0$  if  $\nabla |\mathbf{B}| \neq 0$ . The *standard diffusion* is caused by the second-order derivative of the temperature and is the only diffusion in case the field lines are non-curved, the magnetic field is constant and the diffusion coefficients are constant. The *diffusion variation* term corresponds to the diffusion resulting from a gradient of the diffusion coefficients in the presence of a temperature gradient.

Rewriting the above formulation in  $s, n$  coordinates yields

$$\begin{aligned} \mathcal{A}_1 &= -(D_{\parallel} - D_{\perp}) \mathcal{F}_1 T_n, \\ \mathcal{A}_2 &= (D_{\parallel} - D_{\perp}) \mathcal{F}_2 T_s, \\ \mathcal{A}_3 &= D_{\parallel} T_{ss} + D_{\perp} T_{nn}, \\ \mathcal{A}_4 &= D_{\parallel s} T_s + D_{\perp n} T_n, \end{aligned} \quad (3)$$

where

$$\mathcal{F}_1 = -b_1 b_{2s} + b_2 b_{1s}, \quad \mathcal{F}_2 = -b_2 b_{1n} + b_1 b_{2n}.$$

So we can write

$$\nabla \cdot (\mathbf{D} \cdot \nabla T) = -(D_{\parallel} - D_{\perp}) \mathcal{F}_1 T_n + (D_{\parallel} - D_{\perp}) \mathcal{F}_2 T_s + D_{\parallel} T_{ss} + D_{\perp} T_{nn} + D_{\parallel s} T_s + D_{\perp n} T_n.$$

Note that  $\mathcal{F}_1 = -\alpha_s$  and  $\mathcal{F}_2 = \alpha_n$ , where  $\alpha$  is defined in figure 1.

When applying the equations of magnetohydrodynamics to nuclear fusion plasmas, an assumption often made is that the temperature is diffused instantaneously along the field line, i.e.  $D_{\parallel} = 0$ . This means that the variation of the temperature in the direction of the field line is zero, i.e.,  $\mathbf{b} \cdot \nabla T = 0$ ,  $T_s = 0$ . The terms  $\mathcal{F}_1, \mathcal{F}_2$  in parts  $\mathcal{A}_1, \mathcal{A}_2$  can be approximated in three different ways: I) use an aligned stencil to approximate  $b_{1_s}, b_{1_n}, b_{2_s}, b_{2_n}$ , II) estimation of  $x_{ss}, x_{nn}, y_{ss}, y_{nn}$  by following the field line track, III) apply interpolation of  $b_1, b_2$  to obtain  $b_{1_s}, b_{1_n}, b_{2_s}, b_{2_n}$  directly. We will describe these approaches in sections 3.4.2, 3.4.3 and 3.5 respectively.

### 3.4.1 Interpolation scheme

We continue by applying an aligned stencil to approximate equation (3) using field-aligned stencil points. The stencil points  $r, l, u, d, c$  are given in figure 4. We consider  $x, y$  as local coordinates, where the origin is located in the stencil point  $i, j$ . The values at the locations  $r, l, u, d$  are determined by bi-quadratic interpolation:

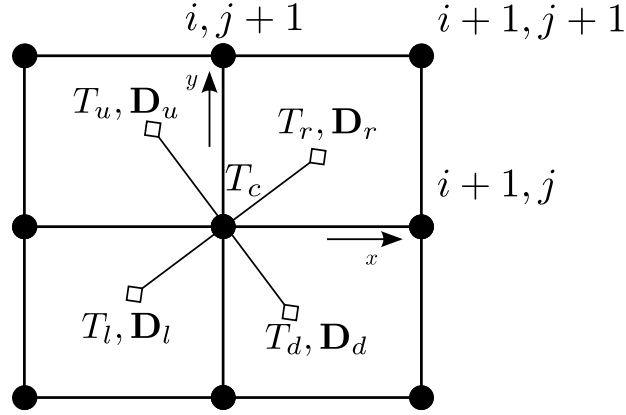


Figure 4: Locally transformed grid, 5-point stencil

$$v(x, y) = c_1 x^2 y^2 + c_2 x^2 y + c_3 y^2 x + c_4 x^2 + c_5 y^2 + c_6 xy + c_7 x + c_8 y + c_9, \quad x, y \in [-h, h], \quad (4)$$

where  $v$  can represent  $T, b_1, b_2, D_{\parallel}$  or  $D_{\perp}$ . For convenience we assume that we have a uniform Cartesian grid with  $\Delta x = \Delta y = h$ . Then, for  $T$ , the coefficients  $c_1, \dots, c_9$  follow from

$$\begin{pmatrix} c_1 \\ c_2 \\ c_3 \\ c_4 \\ c_5 \\ c_6 \\ c_7 \\ c_8 \\ c_9 \end{pmatrix} = \mathbf{V}^{-1} \mathbf{T}, \quad \mathbf{V} = \begin{pmatrix} h^4 & h^3 & -h^3 & h^2 & h^2 & -h^2 & -h & h & 1 \\ h^4 & h^3 & h^3 & h^2 & h^2 & h^2 & h & h & 1 \\ h^4 & -h^3 & -h^3 & h^2 & h^2 & h^2 & -h & -h & 1 \\ h^4 & -h^3 & h^3 & h^2 & h^2 & -h^2 & h & -h & 1 \\ 0 & 0 & 0 & h^2 & 0 & 0 & -h & 0 & 1 \\ 0 & 0 & 0 & h^2 & 0 & 0 & h & 0 & 1 \\ 0 & 0 & 0 & 0 & h^2 & 0 & 0 & h & 1 \\ 0 & 0 & 0 & 0 & h^2 & 0 & 0 & -h & 1 \\ 0 & 0 & 0 & 0 & 0 & 0 & 0 & 0 & 1 \end{pmatrix}, \quad \mathbf{T} = \begin{pmatrix} T_{i-1, j+1} \\ T_{i+1, j+1} \\ T_{i-1, j-1} \\ T_{i+1, j-1} \\ T_{i-1, j} \\ T_{i+1, j} \\ T_{i, j+1} \\ T_{i, j-1} \\ T_{i, j} \end{pmatrix}.$$

The identical relations hold for the coefficients  $c_1, \dots, c_9$  for  $b_1, b_2, D_{\parallel}$  and  $D_{\perp}$ . The matrix  $\mathbf{V}$  contains the polynomial terms for each node, see figure 4. The coefficients  $c_1, \dots, c_9$  are now given by

$$\begin{aligned}
c_1^V &= \frac{1}{h^4} \left( T_{i,j} - \frac{T_{i,j-1}}{2} - \frac{T_{i-1,j}}{2} - \frac{T_{i+1,j}}{2} - \frac{T_{i,j+1}}{2} + \frac{T_{i-1,j-1}}{4} + \frac{T_{i+1,j-1}}{4} + \frac{T_{i+1,j+1}}{4} + \frac{T_{i-1,j+1}}{4} \right), \\
c_2^V &= \frac{1}{4h^3} (2T_{i,j-1} - 2T_{i,j+1} + T_{i-1,j+1} + T_{i+1,j+1} - T_{i-1,j-1} - T_{i+1,j-1}), \\
c_3^V &= \frac{1}{4h^3} (2T_{i-1,j} - 2T_{i+1,j} + T_{i+1,j-1} + T_{i+1,j+1} - T_{i-1,j-1} - T_{i-1,j+1}), \\
c_4^V &= \frac{1}{2h^2} (T_{i-1,j} - 2T_{i,j} + T_{i+1,j}), \quad c_5^V = \frac{1}{2h^2} (T_{i,j-1} - 2T_{i,j} + T_{i,j+1}), \\
c_6^V &= \frac{1}{4h^2} (T_{i-1,j-1} + T_{i+1,j+1} - T_{i+1,j-1} - T_{i-1,j+1}), \\
c_7^V &= \frac{T_{i+1,j} - T_{i-1,j}}{2h}, \quad c_8^V = \frac{T_{i,j+1} - T_{i,j-1}}{2h}, \\
c_9^V &= T_{i,j},
\end{aligned}$$

where the superscript  $V$  denotes *Vandermonde*. Note that the coefficients  $c_1, \dots, c_8$  are all approximations of differential terms in point  $i, j$ ,

$$\begin{aligned}
c_1 &= \frac{1}{4} T_{xxyy} + \mathcal{O}(h^2), \quad c_2 = \frac{1}{2} T_{xxy} + \mathcal{O}(h^2), \quad c_3 = \frac{1}{2} T_{yyx} + \mathcal{O}(h^2), \\
c_4 &= \frac{1}{2} T_{xx} + \mathcal{O}(h^2), \quad c_5 = \frac{1}{2} T_{yy} + \mathcal{O}(h^2), \quad c_6 = T_{xy} + \mathcal{O}(h^2), \\
c_7 &= T_x + \mathcal{O}(h^2), \quad c_8 = T_y + \mathcal{O}(h^2).
\end{aligned} \tag{5}$$

For a spatially constant diffusion tensor the Vandermonde coefficients are similar to the approximation of the respective differential terms for the asymmetric scheme by Günter et al. For comparison purposes we change the coefficients so that they have similar approximation as the symmetric scheme by Günter et al in case of constant diffusion coefficients. Effectively we change the approximations for  $T_x, T_y, T_{xx}$  and  $T_{yy}$  to involve more nodes to approximate the respective differentials,

$$\begin{aligned}
c_4^S &= \frac{1}{8h^2} (T_{i-1,j+1} + T_{i-1,j-1} - 2T_{i,j-1} + 2T_{i-1,j} - 4T_{i,j} + 2T_{i+1,j} - 2T_{i,j+1} + T_{i+1,j+1} + T_{i+1,j-1}), \\
c_5^S &= \frac{1}{8h^2} (T_{i-1,j+1} + T_{i-1,j-1} - 2T_{i-1,j} + 2T_{i,j-1} - 4T_{i,j} + 2T_{i,j+1} - 2T_{i+1,j} + T_{i+1,j+1} + T_{i+1,j-1}), \\
c_7^S &= \frac{1}{8h} (2T_{i+1,j} + T_{i+1,j+1} + T_{i+1,j-1} - 2T_{i-1,j} - T_{i-1,j+1} - T_{i-1,j-1}), \\
c_8^S &= \frac{1}{8h} (2T_{i,j+1} + T_{i-1,j+1} + T_{i+1,j+1} - 2T_{i,j-1} - T_{i-1,i-1} - T_{i+1,j-1}).
\end{aligned}$$

These are second-order accurate approximations of  $T_{xx}, T_{yy}, T_x, T_y$  respectively. This is equivalent to

$$c_4^S = c_4^V + c_1^V \frac{1}{2} h^2, \quad c_5^S = c_5^V + c_1^V \frac{1}{2} h^2, \quad c_7^S = c_7^V + c_3^V \frac{1}{2} h^2, \quad c_8^S = c_8^V + c_2^V \frac{1}{2} h^2,$$

where the superscript  $S$  denotes symmetric. However, when using these coefficients in the bi-quadratic interpolation they do not exactly yield all nodal values for the given locations.

The locations of  $r, l, u, d$  are based on the field line, a first estimate is to apply a single step in the direction of the field line. With  $s$  the coordinate in field line direction,  $n$  the coordinate normal to it and with  $\Delta s$  and  $\Delta n$  the steps in both directions, and defining  $\mathbf{b} = (b_1, b_2)^T$ ,  $\mathbf{b}_{\perp} = (-b_2, b_1)^T$  the locations are given by

$$(x_r, y_r) = \mathbf{b}^T \Delta s, \quad (x_l, y_l) = -\mathbf{b}^T \Delta s, \quad (x_u, y_u) = \mathbf{b}_{\perp} \Delta n, \quad (x_d, y_d) = -\mathbf{b}_{\perp} \Delta n. \tag{6}$$

Now we apply these coordinates (6) to construct discrete schemes in  $s, n$ -coordinates for the individual parts  $\mathcal{A}_1, \mathcal{A}_2, \mathcal{A}_3$  and  $\mathcal{A}_4$ .

### 3.4.2 Accuracy analysis

In the previous section we established two sets of coefficients for a bi-quadratic interpolation scheme. The following analysis holds for a general set of these coefficients, provided the coefficients are second-order accurate approximations of the differential terms given by (5). The superscripts of the coefficients denote the respective variables that are interpolated. We remark that although the accuracy requirement holds for the sum  $\mathcal{A}_1 + \mathcal{A}_2 + \mathcal{A}_3 + \mathcal{A}_4$ , we choose to impose it on  $\mathcal{A}_1, \mathcal{A}_2, \mathcal{A}_3$  and  $\mathcal{A}_4$  individually because we wish to identify the specific terms that cause numerical issues.

For the approximation of  $\mathcal{A}_4$  we have the following expression:

$$\mathcal{A}_4 \approx \frac{D_{\parallel r} - D_{\parallel l}}{2\Delta s} \frac{T_r - T_l}{2\Delta s} + \frac{D_{\perp u} - D_{\perp d}}{2\Delta n} \frac{T_u - T_d}{2\Delta n}. \quad (7)$$

To verify that this scheme approximates part  $\mathcal{A}_4$  second-order accurately we substitute the interpolation functions in equation (7) and we collect the coefficients for zeroth and first-order terms of  $h$ . Noting that  $x_{l,r,u,d}, y_{l,r,u,d}, s, n$  are of order  $h$  we get

$$\begin{aligned} 0^{th}\text{-order: } & \frac{1}{4\Delta s^2} \left( c_7^{D_{\parallel}}(x_r - x_l) + c_8^{D_{\parallel}}(y_r - y_l) \right) \left( c_7^T(x_r - x_l) + c_8^T(y_r - y_l) \right), \\ & \frac{1}{4\Delta n^2} \left( c_7^{D_{\perp}}(x_u - x_d) + c_8^{D_{\perp}}(y_u - y_d) \right) \left( c_7^T(x_u - x_d) + c_8^T(y_u - y_d) \right), \\ 1^{st}\text{-order: } & \frac{1}{4\Delta s^2} \left( c_7^{D_{\parallel}}(x_r - x_l) + c_8^{D_{\parallel}}(y_r - y_l) \right) \left( c_4^T(x_r^2 - x_l^2) + c_5^T(y_r^2 - y_l^2) + c_6^T(x_r y_r - x_l y_l) \right), \\ & \frac{1}{4\Delta n^2} \left( c_7^{D_{\perp}}(x_u - x_d) + c_8^{D_{\perp}}(y_u - y_d) \right) \left( c_4^T(x_u^2 - x_d^2) + c_5^T(y_u^2 - y_d^2) + c_6^T(x_u y_d - x_d y_u) \right). \end{aligned}$$

Now the zeroth-order expression must be equal to  $\mathcal{A}_4$  and the first-order expression must be zero. The requirements that can be distilled from this are

$$\begin{aligned} (x_r - x_l)^2 &= 4b_1^2 \Delta s^2, & (y_r - y_l)^2 &= 4b_2^2 \Delta s^2, & (x_r - x_l)(y_r - y_l) &= 4b_1 b_2 \Delta s^2, \\ (x_u - x_d)^2 &= 4b_2^2 \Delta n^2, & (y_u - y_d)^2 &= 4b_1^2 \Delta n^2, & (x_u - x_d)(y_u - y_d) &= -4b_1 b_2 \Delta n^2, \\ x_{r,u}^2 - x_{l,d}^2 &= 0, & y_{r,u}^2 - y_{l,d}^2 &= 0, & x_{r,u} y_{r,u} - x_{l,d} y_{l,d} &= 0. \end{aligned}$$

This holds for the locations given by equation (6). From this it appears that the term  $\mathcal{A}_4$  can be approximated with second-order accuracy.

For the terms  $\mathcal{A}_3, \mathcal{A}_2, \mathcal{A}_1$  we apply the following finite-difference formulae

$$\mathcal{A}_3 \approx D_{\parallel} \frac{T_r - 2T_c + T_l}{\Delta s^2} + D_{\perp} \frac{T_u - 2T_c + T_d}{\Delta n^2}, \quad (8)$$

$$\mathcal{A}_2 \approx (D_{\parallel} - D_{\perp}) \left( -b_2 \frac{b_{1_u} - b_{1_d}}{2\Delta n} + b_1 \frac{b_{2_u} - b_{2_d}}{2\Delta n} \right) \frac{T_r - T_l}{2\Delta s}, \quad (9)$$

$$\mathcal{A}_1 \approx - (D_{\parallel} - D_{\perp}) \left( -b_1 \frac{b_{2_r} - b_{2_l}}{2\Delta s} + b_2 \frac{b_{1_r} - b_{1_l}}{2\Delta s} \right) \frac{T_u - T_d}{2\Delta n}. \quad (10)$$

Following a similar logic as for  $\mathcal{A}_4$ , substituting the interpolation values in equations (8), (9), (10) and collecting terms of equal order in  $h$  gives second-order accuracy for all terms. We call this method *aligned Vandermonde* or *aligned symmetric* depending on the coefficients. In practice we decrease  $\Delta s$  and  $\Delta n$  with increasing anisotropy, and we may simply and safely take  $\Delta s = \Delta n$ . The construction of the linear operator is described in appendix B.

### 3.4.3 Curvature terms

The aligned schemes presented before assume that the direction does not change from the interpolation point  $l$  up to the interpolation  $r$ , and likewise from interpolation point  $u$  to point  $d$ . Now we consider a numerical

treatment of the terms  $b_{1_s}, b_{1_n}, b_{2_s}, b_{2_n}$  based on field line curvature, so we explicitly allow for curvature to approximate these terms. First we write the terms as

$$b_{1_s} = x_{ss}, \quad b_{1_n} = y_{nn}, \quad b_{2_s} = y_{ss}, \quad b_{2_n} = -x_{nn}.$$

This leads to the following equations for  $\mathcal{F}_1, \mathcal{F}_2$ :

$$\mathcal{F}_1 = -b_1 y_{ss} + b_2 x_{ss}, \quad \mathcal{F}_2 = -b_2 y_{nn} - b_1 x_{nn}.$$

The curvature terms can be approximated by

$$x_{ss} = \frac{x_r + x_l}{\Delta s^2}, \quad y_{ss} = \frac{y_r + y_l}{\Delta s^2}, \quad x_{nn} = \frac{x_u + x_d}{\Delta n^2}, \quad y_{nn} = \frac{y_u + y_d}{\Delta n^2}, \quad (11)$$

where the positions  $r, l, u, d$  are not to be confused with the positions we used for the aligned stencil depicted in figure 4. Given an interpolation function for  $b_1$  and  $b_2$  within the stencil area we can apply tracing to find subsequent points. We go from the center point to the interpolation points  $r, l, u, d$  by applying the (second-order accurate) modified Euler scheme (Heun):

tangential direction:

$$\mathbf{x}_k^* = \mathbf{x}_{k-1} \pm \Delta s^* \mathbf{b}(x_{k-1}, y_{k-1}),$$

$$\mathbf{x}_k = \mathbf{x}_{k-1} \pm \frac{1}{2} \Delta s^* (\mathbf{b}(x_{k-1}, y_{k-1}) + \mathbf{b}(x_k^*, y_k^*)), \quad k = 1, \dots, K,$$

normal direction:

$$\mathbf{x}_k^* = \mathbf{x}_{k-1} \pm \Delta n^* \mathbf{b}_\perp(x_{k-1}, y_{k-1}),$$

$$\mathbf{x}_k = \mathbf{x}_{k-1} \pm \frac{1}{2} \Delta n^* (\mathbf{b}_\perp(x_{k-1}, y_{k-1}) + \mathbf{b}_\perp(x_k, y_k)), \quad k = 1, \dots, K,$$

where  $K$  is the number of sub-steps  $\Delta s^*, \Delta n^*$ , and where  $x_0 = y_0 = 0$  (see figure 5). The values  $\Delta s = K \Delta s^*$  and  $\Delta n = K \Delta n^*$  are used in equation (11). Repeatedly stepping in  $s, n$ -direction and applying the

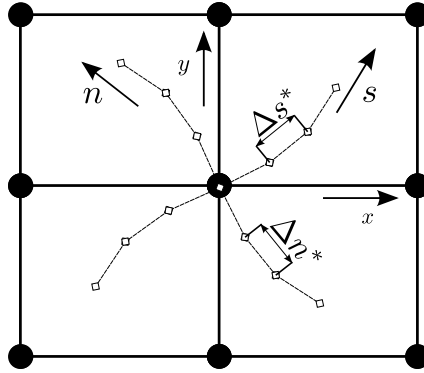


Figure 5: Approximate track of field line and perpendicular curve

interpolation of  $\mathbf{b}$  increases the computational cost. The benefit is that we can easily control the accuracy with which we follow the field line, simply by changing the number of tracing steps.

The current tracing method is expected to be more accurate in determining the curvature terms than the aligned stencil since it follows the actual field line more closely.

### 3.4.4 Bi-linear interpolation per quadrant

For the aligned method we use a bi-quadratic interpolation scheme where we apply all nine stencil points for the determination of the values in aligned stencil points. Here we shortly consider a quadrant-wise bi-linear

interpolation with the location of the central node set to the center point  $(i, j)$ . This gives

$$\begin{aligned}
T_{l,r,u,d} &= ax_{l,r,u,d}y_{l,r,u,d} + bx_{l,r,u,d} + cy_{l,r,u,d} + d, \\
T_r : \quad d &= T_{i,j}, \quad c = \frac{T_{i,j+1} - T_{i,j}}{y_{i,j+1} - y_{i,j}}, \quad b = \frac{T_{i+1,j} - T_{i,j}}{x_{i+1,j} - x_{i,j}}, \quad a = \frac{T_{i+1,j+1} - bdx - cdy - d}{(x_{i+1,j} - x_{i,j})(y_{i,j+1} - y_{i,j})}, \\
T_l : \quad d &= T_{i,j}, \quad c = \frac{T_{i,j} - T_{i,j-1}}{y_{i,j} - y_{i,j-1}}, \quad b = \frac{T_{i,j} - T_{i-1,j}}{x_{i,j} - x_{i-1,j}}, \quad a = \frac{T_{i-1,j-1} - bdx - cdy - d}{(x_{i,j} - x_{i-1,j})(y_{i,j} - y_{i,j-1})}, \\
T_u : \quad d &= T_{i,j}, \quad c = \frac{T_{i,j+1} - T_{i,j}}{y_{i,j+1} - y_{i,j}}, \quad b = \frac{T_{i,j} - T_{i-1,j}}{x_{i,j} - x_{i-1,j}}, \quad a = -\frac{T_{i-1,j+1} - bdx - cdy - d}{(x_{i,j} - x_{i-1,j})(y_{i,j+1} - y_{i,j})}, \\
T_d : \quad d &= T_{i,j}, \quad c = \frac{T_{i,j} - T_{i,j-1}}{y_{i,j} - y_{i,j-1}}, \quad b = \frac{T_{i+1,j} - T_{i,j}}{x_{i+1,j} - x_{i,j}}, \quad a = -\frac{T_{i+1,j-1} - bdx - cdy - d}{(x_{i+1,j} - x_{i,j})(y_{i,j} - y_{i,j-1})}.
\end{aligned}$$

Just considering the differentiation of the second-order terms in parallel direction we get

$$\begin{aligned}
u_{ss} \approx \frac{1}{h^2} &[-2u_{i,j}(b_1 + b_2 - b_1b_2) + u_{i+1,j}(b_1 - b_1b_2) + u_{i-1,j}(b_1 - b_1b_2) + u_{i,j+1}(b_2 - b_1b_2) \\
&+ u_{i,j-1}(b_2 - b_1b_2) + (u_{i+1,j+1} + u_{i-1,j-1})b_1b_2].
\end{aligned}$$

Writing out the fourth-order Taylor expansion of the parallel diffusion  $u_{ss}$ , assuming constant diffusion coefficients, gives

$$u_{ss} = b_1u_{xx} + b_2u_{yy} + 2b_1b_2u_{xy} + \mathcal{O}(h^2).$$

This is not consistent with the analytic form; we have  $b_1$  and  $b_2$  instead of  $b_1^2$  and  $b_2^2$  respectively. This inconsistency is due to the fact that bi-linear interpolation is used and so the directions are only inserted with first-order accuracy. The downside of quadrant-wise bi-linear interpolation is that one has to track in which quadrant the stencil point is to apply the appropriate interpolation.

### 3.5 Exact differentiation after interpolation

We can also find a direct approximation of the various spatial derivatives involved in the anisotropic diffusion operator, by writing the interpolation function (4) in terms of  $s, n$  and by taking the appropriate derivatives of this rewritten function. Then, the interpolation functions for  $b_1$  and  $b_2$  need to be applied to find the final form of the approximation. We use the non-conservative form

$$T_t = D_{\parallel}v_{ss}^T + D_{\perp}v_{nn}^T + v_s^{D_{\parallel}}v_s^T + v_n^{D_{\perp}}v_n^T + (D_{\parallel} - D_{\perp})(Sv_s^T - Nv_n^T),$$

where the terms with  $v$  represent the derivatives of the bi-quadratic interpolation functions for the quantities denoted by the superscript, i.e.,  $v^T$  is the interpolation function for the temperature. The first-order differentials are written as

$$v_s^{D_{\parallel}}v_s^T + v_n^{D_{\perp}}v_n^T = (c_7^T b_1 + c_8^T b_2)(c_7^{D_{\parallel}} b_1 + c_8^{D_{\parallel}} b_2) + (-c_7^T b_2 + c_8^T b_1)(-c_7^{D_{\perp}} b_2 + c_8^{D_{\perp}} b_1).$$

The diffusive terms are given by

$$D_{\parallel}v_{ss}^T + D_{\perp}v_{nn}^T = 2D_{\parallel}(c_4b_1^2 + c_5b_2^2 + c_6b_1b_2) + 2D_{\perp}(c_4b_2^2 + c_5b_1^2 - c_6b_1b_2),$$

and the curvature-dependent terms by

$$\begin{aligned}
(D_{\parallel} - D_{\perp})(Sv_s^T - Nv_n^T) &= 2D_{\parallel} \left[ c_7 \left( b_1c_7^{b_1} + \frac{1}{2}b_1c_8^{b_2} + \frac{1}{2}b_2c_8^{b_1} \right) + c_8 \left( b_2c_8^{b_2} + \frac{1}{2}b_2c_7^{b_1} + \frac{1}{2}b_1c_7^{b_2} \right) \right] + \\
&2D_{\perp} \left[ c_7 \left( b_2c_7^{b_2} - \frac{1}{2}b_1c_8^{b_2} - \frac{1}{2}b_2c_8^{b_1} \right) + c_8 \left( b_1c_8^{b_1} - \frac{1}{2}b_2c_7^{b_1} - \frac{1}{2}b_1c_7^{b_2} \right) \right].
\end{aligned}$$

The geometric term is recursive since  $b_1, b_2$  depend on  $x, y$  which in turn depend on  $b_1, b_2$ . The aligned finite-difference scheme is identical to the interpolation scheme for  $\Delta s, \Delta n \rightarrow 0$ , see appendix A.

We call these methods *interp. Vandermonde* or *interp. symmetric*, depending on the coefficients that are used. Summarizing, we apply the following methods

- *asymmetric scheme, G. et al.*,
- *symmetric scheme, G. et al.*,
- *aligned Vandermonde/symmetric scheme*,
- *interp. Vandermonde/symmetric scheme*.

## 4 Numerical results

In this section we show the results for several steady test cases. For all the test cases, we have  $\frac{\partial T}{\partial t} = 0$  and the source function  $f$  is such that it produces the exact solution which is given for each test case. We use Dirichlet boundary conditions with the boundary value determined by the assumed solution. As we assume that the time derivative is zero we can assume that in all the test cases  $\mathbf{b} \cdot \nabla T = 0$ .

### 4.1 Constant angle of misalignment

As an initial test we consider a simple steady diffusion problem. The imposed exact solution reads:

$$T(x, y) = xy [\sin(\pi x) \sin(\pi y)]^\gamma, \quad x, y \in [0, 1],$$

where  $\gamma$  is large and where the angle of misalignment  $\alpha$  is set to a constant value. The solution simulates a temperature peak. Computational results for this test case are given in figure 6. The error norm is defined

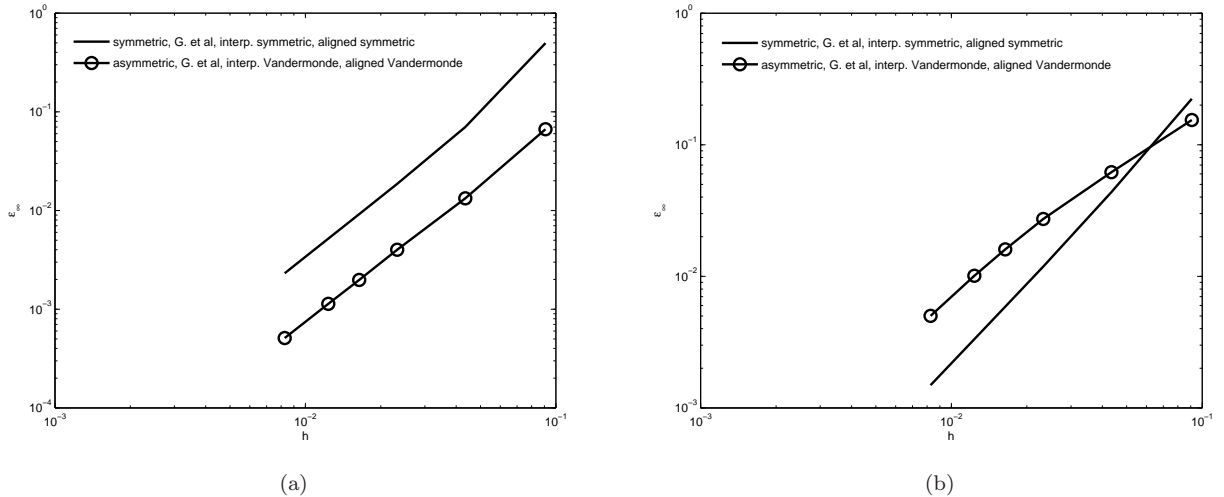


Figure 6: Error  $\epsilon_\infty$  for test cases with constant angles of misalignment,  $\gamma = 10$ ,  $\zeta = 10^9$ , at varying mesh width, (a)  $\alpha = 5^\circ$ , (b)  $\alpha = 30^\circ$ . In the plots all symmetric schemes overlap and likewise do all asymmetric schemes

by

$$\epsilon_\infty = \frac{|\tilde{T} - T|_{max}}{T_{max}},$$

where  $\tilde{T}$  is the approximate temperature. It is clear from the figure that the symmetric schemes conserve the order of accuracy independent of the anisotropy and angle of misalignment. The co-located schemes are only slightly less accurate than the staggered schemes. For larger values, the asymmetric schemes are less than second-order convergent on coarse grids, but they regain second-order convergence on finer grids.

## 4.2 Varying angle of misalignment

Again the problem is considered on a square domain, this time described by  $-0.5 \leq x, y \leq 0.5$ . The following steady-state solution is assumed on the domain

$$T(x, y) = 1 - [(x - x_c)^2 + (y - y_c)^2]^{3/2},$$

with  $x_c = y_c = 0$  for the closed field line case and  $x_c = y_c = 0.5$  for the open field line case. The direction of the parallel diffusion is given by

$$\mathbf{b} = \frac{1}{\sqrt{(x - x_c)^2 + (y - y_c)^2}} \begin{pmatrix} -(y - y_c) \\ x - x_c \end{pmatrix}. \quad (12)$$

Note that both  $\nabla \cdot \mathbf{b}$  and  $\mathbf{b} \cdot \nabla T$  are zero, this means that the term  $\mathcal{A}_2$  comes into play only due to numerical errors, term  $\mathcal{A}_4$  is zero exactly since  $\nabla D_{\parallel}, \nabla D_{\perp}$  are zero. So test case 2 stresses terms  $\mathcal{A}_1$  and  $\mathcal{A}_3$ , with added contribution due to numerical errors in term  $\mathcal{A}_2$ .

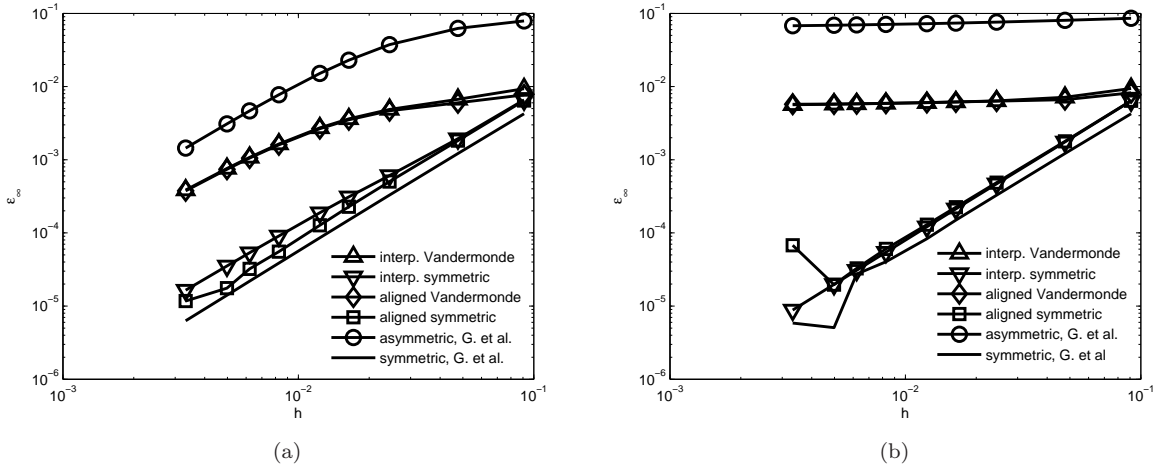


Figure 7: Error  $\epsilon_\infty$  for test cases with varying misalignment, (a)  $\zeta = 10^3$ , (b)  $\zeta = 10^9$

We study the accuracy of the various schemes for two anisotropic cases, one being extremely anisotropic,  $\zeta = 10^9$ , both with  $x_c = y_c = 0$ . We observe from figure 7 that for the extremely anisotropic case our aligned symmetric scheme and our interpolated symmetric scheme preserve their second-order of accuracy. All other schemes fail completely; they are all inconsistent for the  $\zeta = 10^9$  test case.

A detail to be observed from figure 7 is that for extremely high levels of anisotropy the symmetric scheme of Günter et al and the current symmetric schemes show a wiggle in the error convergence. This is partly

caused by the fact that the linear operator becomes ill-conditioned for  $h \rightarrow 0$  with a condition number of order  $10^{13}$  and partly by the fact that in the origin  $\mathbf{b}$  is undefined for this particular test problem, shifting the origin by a small value  $\epsilon$  of order  $10^{-16}$  removes the wiggle. Günter et al. [30] had problems with number representation for a fourth-order mimetic finite-difference scheme. They resolved this by increasing the number representation accuracy. Further, it can be shown that the analytic problem becomes ill-posed for  $\zeta \rightarrow \infty$  (see Degond et al. [16]). The asymmetric scheme is not suffering from number representation errors here. However this is probably due to the solution not being close enough to the limit solution.

Finally, in figure 8 we make a more extensive study of the behavior of the different schemes at varying anisotropy. Here the interpolated symmetric scheme and aligned symmetric scheme perform slightly better than the symmetric scheme by Günter et al.; their errors do not increase with increasing anisotropy.

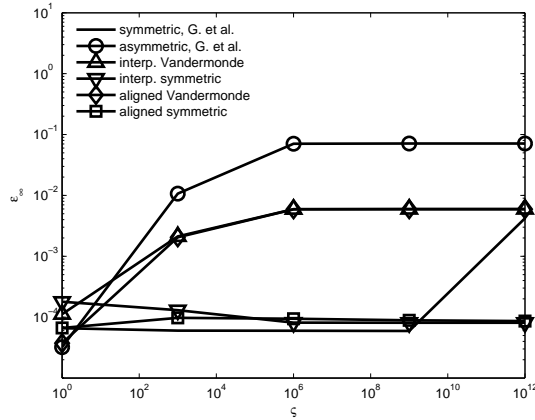


Figure 8:  $\epsilon_\infty$ -error norm versus the anisotropy  $\zeta$  for a  $100 \times 100$  grid

The aligned scheme and the interpolation scheme perform equally well as the symmetric scheme by Günter et al in terms of anisotropy independence of the error, see figure 8. Starting from an anisotropy ratio of  $\zeta = 10^9$  the symmetric scheme by Günter et al begins to deteriorate. This is most likely due to ill-conditioning of the linear operator. The fact that the symmetric scheme by Günter et al suffers from ill-conditioning for extreme values of the level of anisotropy is an indication that the parallel and perpendicular components are numerically strictly separated. For  $\zeta \rightarrow \infty$  equation (1) in combination with Dirichlet and Neumann boundary conditions becomes ill-posed due to the fact that  $\nabla \cdot (D_{\parallel} \mathbf{b} \cdot \nabla T \mathbf{b}) = 0$  has infinitely many solutions. Vice versa, the fact that the asymmetric scheme by Günter et al does not suffer from ill-conditioning of the linear operator is an indication that for  $\zeta \rightarrow \infty$  the approximation does not approach the limit solution of (1).

Setting  $D_{\parallel}$  to zero enforces that  $\mathbf{q}_{\parallel} = 0$  in the  $t \rightarrow \infty$  limit, this restores the accuracy of the aligned methods. The aligned Vandermonde and the interpolated Vandermonde method are now close to second-order accuracy. The order of accuracy for the aligned symmetric method and the interpolated symmetric method are slightly decreased below second order.

Running the test case with  $x_c = y_c = 0.5$  gives second-order convergence for all schemes. The qualitative difference between  $x_c = y_c = 0$  and  $x_c = y_c = 0.5$  is the presence of a singular point in the latter case, a point where the direction vector  $\mathbf{b}$  is undefined and over which the vector changes discontinuously.

We suspect that the accuracy of the symmetric scheme by Günter et al. has some dependency on the symmetry of the problem, this is investigated in section 4.3.

For the following four test cases we dismiss the asymmetric scheme by Günter et al and the aligned and interpolated schemes with Vandermonde coefficients, since for this particular test case they show near zeroth-order convergence for high values of anisotropy.

### 4.3 Tilted elliptic temperature distributions

So far we have used forcing functions that are spatially symmetric. Now we apply a forcing function that gives the solution for a tilted elliptic temperature distribution. This distribution has no symmetry axes aligned with the coordinate axes. The first tilted elliptic distribution has no closed field lines. Basically, the field lines go in the same general direction, see figure 9a.

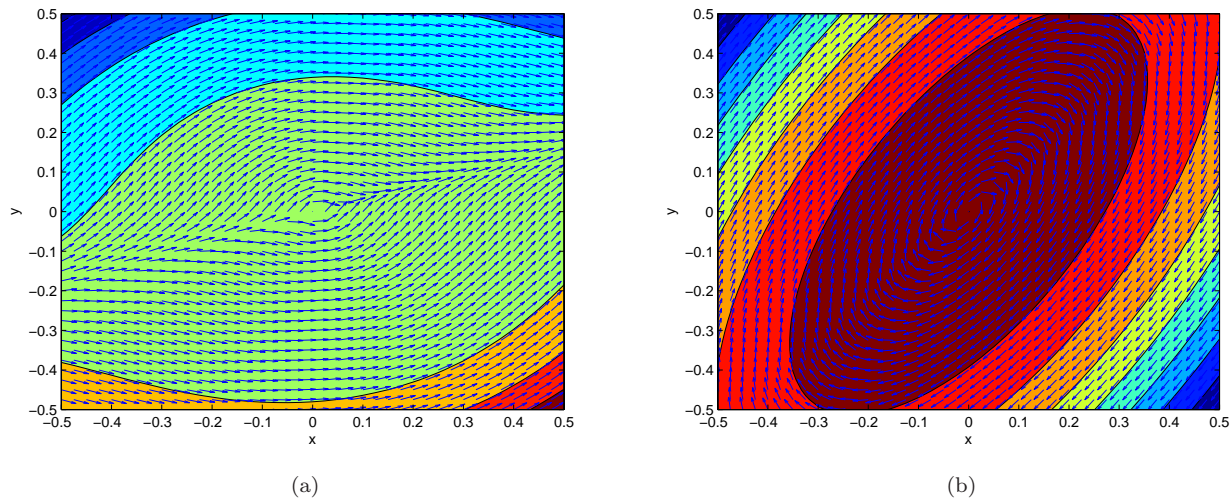


Figure 9: Tilted test cases, field line direction with (a) non-rotating field lines,  $a = 25, b = -75$ , (b) closed field lines,  $a = 0.15, b = 0.85$

The exact solution is given by

$$T(x, y) = 1 + (ax + by)(x^2 + y^2)^{3/2}, \quad \mathbf{b} = \frac{1}{\sqrt{T_x^2 + T_y^2}} \begin{pmatrix} -T_y \\ T_x \end{pmatrix}, \quad x, y \in [-0.5, 0.5].$$

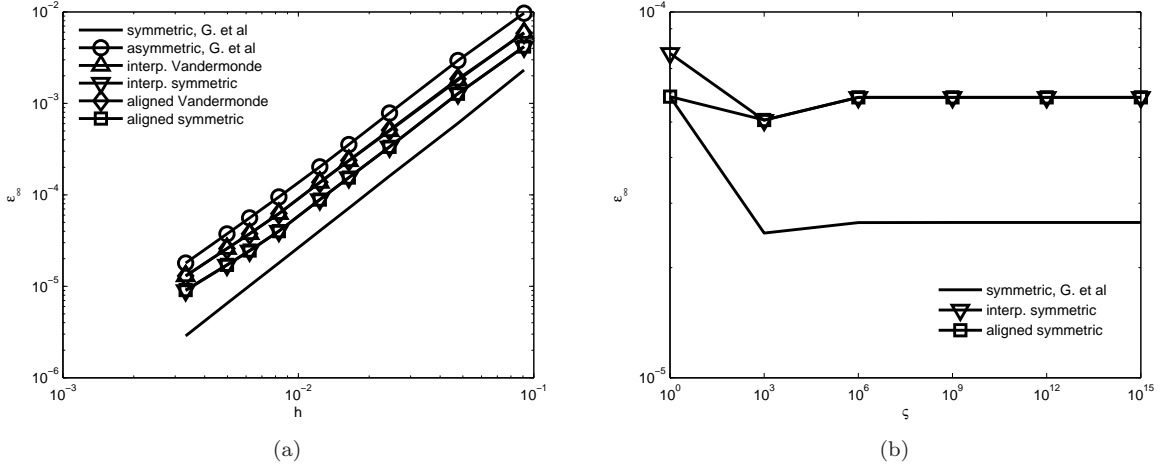


Figure 10:  $a = 25, b = -75$ , (a)  $\epsilon_\infty$  convergence for  $\zeta = 10^9$ , (b)  $\epsilon_\infty$ -error norm versus the anisotropy  $\zeta$  for a  $100 \times 100$  grid

In figure 10 we present numerical results. We see that all three schemes considered are very similar in performance, maintaining order of convergence and having similar accuracy. In the origin of the domain both  $b_1$  and  $b_2$  go to zero. So the unit direction vector is undefined there. However, the unit direction vector is continuous in all directions through the origin.

The distribution for the second tilted test case is given by

$$T(x, y) = 1 - (a^2(x \cos \theta + y \sin \theta)^2 + b^2(x \sin \theta - y \cos \theta)^2)^{3/2}, \quad x, y \in [-0.5, 0.5], \quad (13)$$

with  $\mathbf{b}$  as before, Distribution (13) is qualitatively similar to the distribution shown in figure 9b.

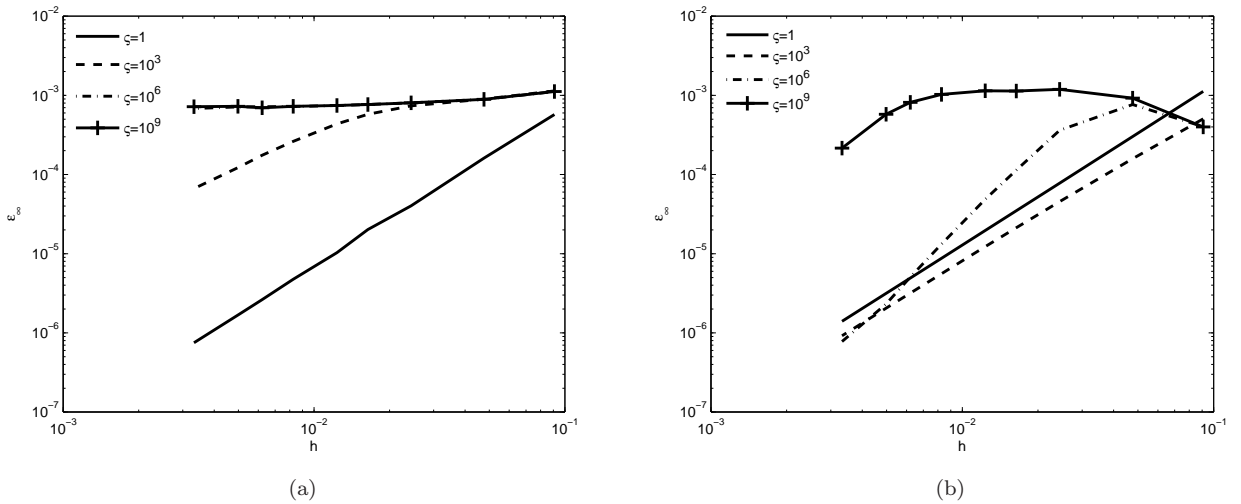


Figure 11: Second tilted test case, convergence plots for several levels of anisotropy with  $a = 0.15, b = 0.85, \theta = \pi/3$ , (a) aligned symmetric scheme, (b) symmetric scheme by Günter et al

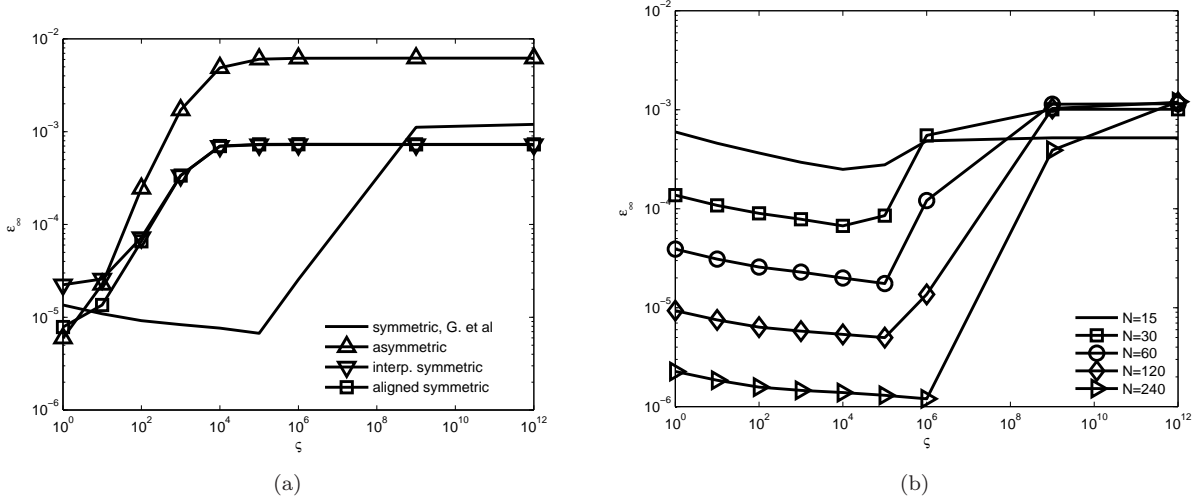


Figure 12: Second tilted test case, accuracy plot for several levels of anisotropy with  $a = 0.15$ ,  $b = 0.85$ ,  $\theta = \pi/3$  with a grid size of  $100 \times 100$ , (a) aligned symmetric scheme, (b) symmetric scheme by Günter et al

The tilted test case shows that none of the investigated second-order schemes is able to approximate anisotropic diffusion whilst maintaining formal accuracy globally independent of the level of anisotropy. The last test case has closed field lines.

#### 4.4 Temperature-dependent diffusion coefficients

Until now we have not treated part  $\mathcal{A}_4$  of the diffusion equation. To do this we describe the coefficients by

$$D_{\parallel} = c_{\parallel} T^{5/2}, \quad D_{\perp} = c_{\perp} T^{-1/2}.$$

These expressions are representative of actual MHD-simulations for fusion plasmas except for the absence of density. We apply temperature dependence of the diffusion coefficients to the test case described in section 4.2. From the results shown in figure 13a we see that the aligned symmetric method and the interpolated symmetric method maintain second-order convergence independent of the anisotropy whereas the symmetric method by Günter et al now has reduced convergence. There is no qualitative difference between using a harmonic mean and an arithmetic mean. This is probably due to the smoothness of the solution.

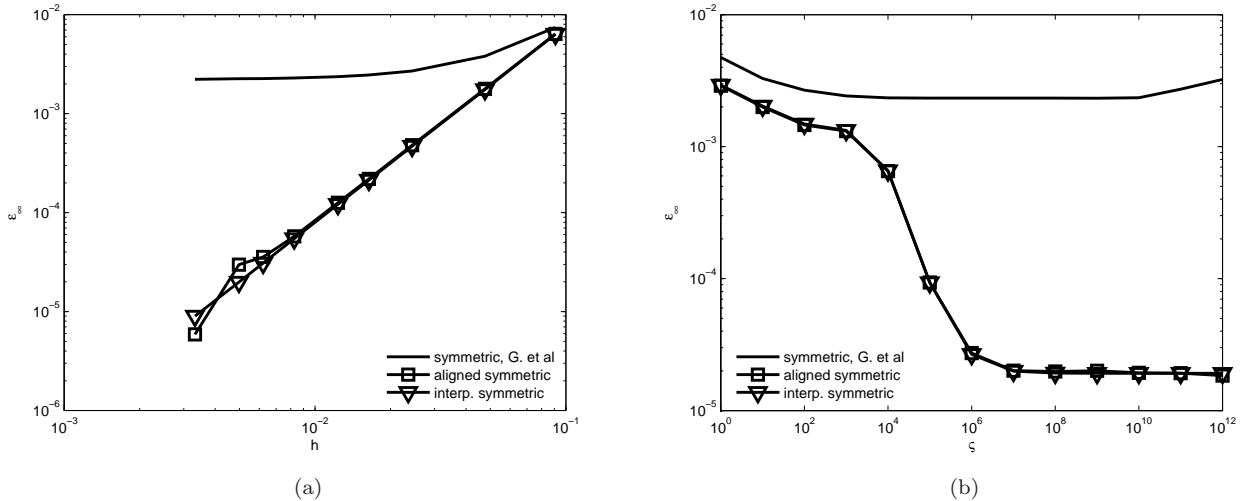


Figure 13: Test case 1 with temperature-dependent diffusion coefficients,  $\epsilon_\infty$ -error, (a) convergence for  $\zeta = 10^9$ , (b) dependence on anisotropy for a  $100 \times 100$  grid

The reason for the loss of performance for the symmetric scheme of Günter et al. is that instead of having diffusion tensor values exactly on the dual grid we now have to interpolate between the primal grid points.

An obvious way to prevent the need for interpolation is to define the temperature on both the primal and the dual grid, i.e. favoring the DDFV and the FECC methods in case of temperature dependent diffusion coefficients.

## 5 Conservation error

The schemes we present in the current work discretize the non-conservative form of the diffusion equation. To quantify the effect of non-conservation we apply the current interp. symmetric scheme and the symmetric scheme of Günter et al., to an unsteady test problem with zero source terms and Neumann boundary conditions. For the time integration we use the Crank-Nicolson scheme with the time step chosen such that the time integration error is negligible. In this problem we assume that  $\mathbf{q}_\perp = 0$ , so any perpendicular diffusion is numerical. We define the global conservation error at time level  $n$  as

$$\epsilon_T = 1/N \left| \sum_k^N T_{k,n} - \sum_k^N T_{k,0} \right|,$$

where  $k$  refers to the  $k$ -th component of the solution vector and where  $N$  is the number of unknowns. As a test case we consider the diffusion of a Gaussian initial distribution

$$T(x, y, t = 0) = \exp(-r^2/2\sigma^2), \quad r^2 = (x - d)^2 + (y - d)^2, \quad x, y \in [-0.5, 0.5],$$

with  $\sigma = 0.05$ . The direction of diffusion  $\mathbf{b}$  is given by

$$\mathbf{b} = \frac{1}{\sqrt{(x - x_0)^2 + (y - y_0)^2}} \begin{pmatrix} -(y - y_0) \\ x - x_0 \end{pmatrix}.$$

The Gaussian distribution is diffused along the circular field lines. We consider a closed field lines case, with  $x_0 = y_0 = 0$ .

Regarding the implementation of the boundary conditions: for the symmetric scheme by Günter et al. the flux points are placed exactly on the boundary. For the current co-located schemes the temperature and the flux quantities are located in the same points. The implementation of the Neumann boundary conditions for the current scheme is done by using ghost points.

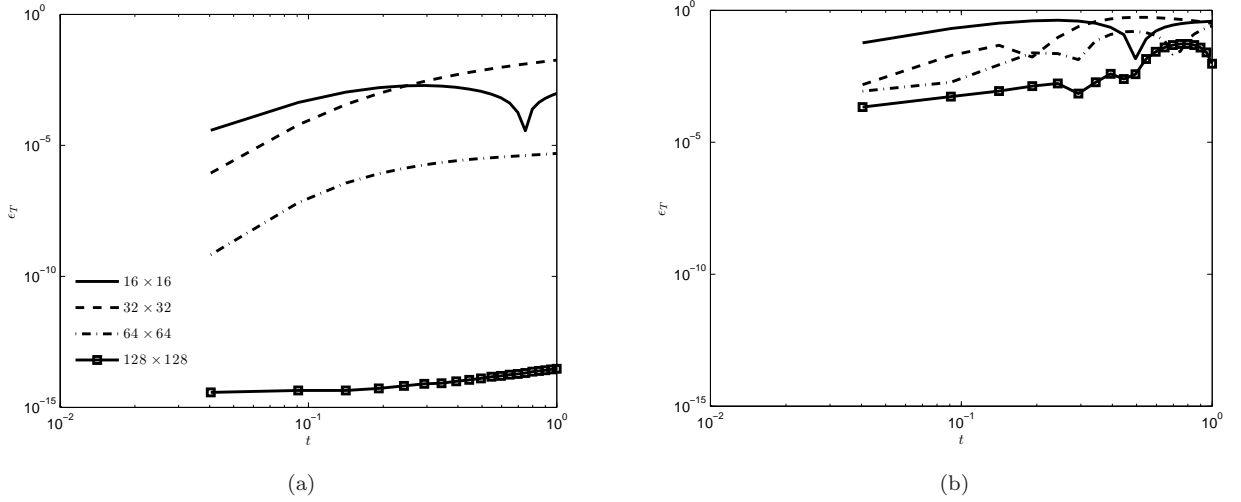


Figure 14:  $\epsilon_T$  error of the symmetric scheme for two-dimensional diffusion test case with a Gaussian initial distribution,  $D_{\perp} = 0, \sigma = 0.05, t_{end} = 1, d = 0.25, x, y \in [-2, 2]$ , (a) symmetric, G. et al, (b) interp. symmetric

From the results shown in figures 14a we see that both schemes are not conservative, the interpolation scheme with symmetric coefficients being most non-conservative.

## 5.1 Aligned gradient operator

Starting from the symmetric scheme by Günter et al we consider an aligned stencil for each gradient. We leave the operator for the divergence untouched. Originally in each flux point  $\mathbf{D}\nabla T$  is approximated by

$$\mathbf{D}\nabla T|_{i+1/2, j+1/2} \approx \left[ D_{11} \frac{T_{i+1, j+1} + T_{i+1, j} - T_{i, j+1} - T_{i, j}}{2h} \quad D_{12} \frac{T_{i+1, j+1} + T_{i+1, j} - T_{i, j+1} - T_{i, j}}{2h} \right]^T + \left[ D_{21} \frac{T_{i+1, j+1} + T_{i+1, j} - T_{i, j+1} - T_{i, j}}{2h} \quad D_{22} \frac{T_{i+1, j+1} + T_{i+1, j} - T_{i, j+1} - T_{i, j}}{2h} \right]^T,$$

and likewise for the other flux points, this can be written as

$$\mathbf{D}^*(\mathbf{b} \cdot \nabla T), \quad \mathbf{D}^* = \begin{pmatrix} D_{\parallel}(b_1 + b_2) - D_{\perp} b_2 & D_{\perp}(b_2 - b_1) + D_{\parallel} b_1 \\ D_{\perp}(b_2 - b_1) + D_{\parallel} b_2 & D_{\parallel}(b_1 + b_2) - D_{\perp} b_1 \end{pmatrix}.$$

Now we approximate  $\mathbf{b} \cdot \nabla T$  by applying an aligned stencil in combination with a bilinear interpolation of the four surrounding points. The bilinear interpolation  $\tilde{T}(x, y)$  for a flux point  $(i + 1/2, j + 1/2)$  is given by

$$\tilde{T}(x, y)_{i+1/2, j+1/2} = xy(T_{xy})_{i+1/2, j+1/2} + x(T_x)_{i+1/2, j+1/2} + y(T_y)_{i+1/2, j+1/2} + \bar{T}_{i+1/2, j+1/2},$$

and similarly for the other flux points. The coefficients in these bilinear interpolations are given by

$$\begin{aligned} (T_{xy})_{i+1/2,j+1/2} &\approx \frac{T_{i+1,j+1} + T_{i,j} - T_{i+1,j} - T_{i,j+1}}{h^2}, \\ (T_x)_{i+1/2,j+1/2} &\approx \frac{T_{i+1,j+1} + T_{i+1,j} - T_{i,j} - T_{i,j+1}}{h^2}, \\ (T_y)_{i+1/2,j+1/2} &\approx \frac{T_{i+1,j+1} + T_{i,j+1} - T_{i,j} - T_{i+1,j}}{h^2}, \\ \bar{T}_{i+1/2,j+1/2} &= \frac{T_{i+1,j+1} + T_{i+1,j} + T_{i,j+1} + T_{i,j}}{4}, \end{aligned}$$

and similarly for the other flux points. In each flux point we now step in the direction and counter-direction

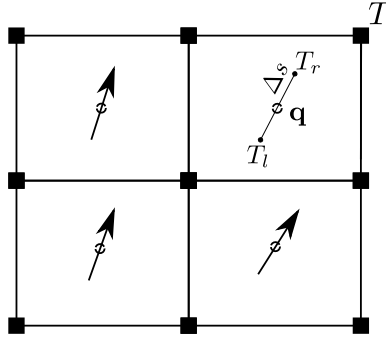


Figure 15: Conservative aligned difference

of  $\mathbf{b}$  with some stepsize  $\Delta s$  and obtain a central difference approximation for the aligned gradient  $\mathbf{b} \cdot \nabla T$ , see figure 15. The resulting approximation is

$$\mathbf{b} \cdot \nabla T|_{i+1/2,j+1/2} = b_1(T_x)_{i+1/2,j+1/2} + b_2(T_y)_{i+1/2,j+1/2},$$

which is the symmetric scheme by Günter et al. that we started with. So we conclude that the symmetric scheme is aligned by construction.

## 5.2 Aligned divergence operator

If we use a nine point interpolation for the temperature we lose conservation. Instead we consider a weighted average of the symmetric gradient approximations. We can obtain a suitable description of the local derivatives by defining the approximations for  $T_x$  and  $T_y$  as

$$\begin{aligned} T_x &\approx \alpha_{ru} \frac{T_{i+1,j+1} + T_{i+1,j} - T_{i,j+1} - T_{i,j}}{2h} + \alpha_{lu} \frac{T_{i,j} + T_{i,j+1} - T_{i-1,j+1} - T_{i-1,j}}{2h} \\ &\quad + \alpha_{ld} \frac{T_{i,j} + T_{i,j-1} - T_{i-1,j} - T_{i-1,j-1}}{2h} + \alpha_{rd} \frac{T_{i+1,j} + T_{i+1,j-1} - T_{i,j} - T_{i,j-1}}{2h}, \\ T_y &\approx \alpha_{ru} \frac{T_{i+1,j+1} + T_{i,j+1} - T_{i,j} - T_{i+1,j}}{2h} + \alpha_{lu} \frac{T_{i,j+1} + T_{i-1,j+1} - T_{i-1,j} - T_{i,j}}{2h} \\ &\quad + \alpha_{ld} \frac{T_{i,j} + T_{i-1,j} - T_{i-1,j-1} - T_{i,j-1}}{2h} + \alpha_{rd} \frac{T_{i+1,j} + T_{i,j} - T_{i,j-1} - T_{i+1,j-1}}{2h}, \end{aligned}$$

with a bilinear description for each  $\alpha$ , and with the conditions

$$\begin{aligned}
\alpha_{ru}\left(\frac{h}{2}, \frac{h}{2}\right) &= 1, & \alpha_{ru}\left(-\frac{h}{2}, \frac{h}{2}\right) &= 0, & \alpha_{ru}\left(\frac{h}{2}, -\frac{h}{2}\right) &= 0, & \alpha_{ru}\left(-\frac{h}{2}, -\frac{h}{2}\right) &= 0, \\
\alpha_{lu}\left(\frac{h}{2}, \frac{h}{2}\right) &= 0, & \alpha_{lu}\left(-\frac{h}{2}, \frac{h}{2}\right) &= 1, & \alpha_{lu}\left(\frac{h}{2}, -\frac{h}{2}\right) &= 0, & \alpha_{lu}\left(-\frac{h}{2}, -\frac{h}{2}\right) &= 0, \\
\alpha_{rd}\left(\frac{h}{2}, \frac{h}{2}\right) &= 0, & \alpha_{rd}\left(-\frac{h}{2}, \frac{h}{2}\right) &= 0, & \alpha_{rd}\left(\frac{h}{2}, -\frac{h}{2}\right) &= 1, & \alpha_{rd}\left(-\frac{h}{2}, -\frac{h}{2}\right) &= 0, \\
\alpha_{ld}\left(\frac{h}{2}, \frac{h}{2}\right) &= 0, & \alpha_{ld}\left(-\frac{h}{2}, \frac{h}{2}\right) &= 0, & \alpha_{ld}\left(\frac{h}{2}, -\frac{h}{2}\right) &= 0, & \alpha_{ld}\left(-\frac{h}{2}, -\frac{h}{2}\right) &= 1.
\end{aligned}$$

We get the following bilinear descriptions

$$\begin{aligned}
\alpha_{ru} &= 1 + \left(\frac{x}{h} - \frac{1}{2}\right) + \left(\frac{y}{h} - \frac{1}{2}\right) + \left(\frac{x}{h} - \frac{1}{2}\right) \left(\frac{y}{h} - \frac{1}{2}\right), \\
\alpha_{lu} &= 1 - \left(\frac{x}{h} + \frac{1}{2}\right) + \left(\frac{y}{h} - \frac{1}{2}\right) - \left(\frac{x}{h} + \frac{1}{2}\right) \left(\frac{y}{h} - \frac{1}{2}\right), \\
\alpha_{rd} &= 1 + \left(\frac{x}{h} - \frac{1}{2}\right) - \left(\frac{y}{h} + \frac{1}{2}\right) - \left(\frac{x}{h} - \frac{1}{2}\right) \left(\frac{y}{h} + \frac{1}{2}\right), \\
\alpha_{ld} &= 1 - \left(\frac{x}{h} + \frac{1}{2}\right) - \left(\frac{y}{h} + \frac{1}{2}\right) + \left(\frac{x}{h} + \frac{1}{2}\right) \left(\frac{y}{h} + \frac{1}{2}\right),
\end{aligned} \tag{14}$$

which also fulfills the consistency requirement that  $\sum \alpha = 1$ . Note that we also have the following properties for the coefficients

$$\begin{aligned}
\alpha_{ru}\left(\frac{h}{2}, 0\right) &= 1/2, & \alpha_{ru}\left(0, \frac{h}{2}\right) &= 1/2, & \alpha_{ru}\left(x, -\frac{h}{2}\right) &= 0, & \alpha_{ru}\left(-\frac{h}{2}, y\right) &= 0, \\
\alpha_{lu}\left(\frac{h}{2}, y\right) &= 0, & \alpha_{lu}\left(0, \frac{h}{2}\right) &= 1/2, & \alpha_{lu}\left(x, -\frac{h}{2}\right) &= 0, & \alpha_{lu}\left(-\frac{h}{2}, 0\right) &= 1/2, \\
\alpha_{rd}\left(\frac{h}{2}, 0\right) &= 1/2, & \alpha_{rd}\left(x, \frac{h}{2}\right) &= 0, & \alpha_{rd}\left(0, -\frac{h}{2}\right) &= 1/2, & \alpha_{rd}\left(-\frac{h}{2}, y\right) &= 0, \\
\alpha_{ld}\left(\frac{h}{2}, y\right) &= 0, & \alpha_{ld}\left(x, \frac{h}{2}\right) &= 0, & \alpha_{ld}\left(0, -\frac{h}{2}\right) &= 1/2, & \alpha_{ld}\left(-\frac{h}{2}, 0\right) &= 1/2.
\end{aligned}$$

We call these coefficients *local symmetric*. When using these coefficients in the bi-quadratic interpolation they do not exactly yield all nodal values for the given locations since it is not an approximation of the temperature but rather a weighted summation of gradients. In this manner we approximate the diffusion equation in conservative form with the divergence written in local coordinates

$$\begin{aligned}
T_t &= \left(b_1 \frac{\partial}{\partial s} - b_2 \frac{\partial}{\partial n}\right) (D_{11}T_x + D_{21}T_y) + \left(b_2 \frac{\partial}{\partial s} + b_1 \frac{\partial}{\partial n}\right) (D_{21}T_x + D_{22}T_y) + f \Rightarrow \\
T_t &\approx b_1 \frac{(D_{11}T_x + D_{21}T_y)_r - (D_{11}T_x + D_{21}T_y)_l}{2\Delta s} - b_2 \frac{(D_{11}T_x + D_{21}T_y)_u - (D_{11}T_x + D_{21}T_y)_d}{2\Delta n} \\
&\quad + b_2 \frac{(D_{21}T_x + D_{22}T_y)_r - (D_{21}T_x + D_{22}T_y)_l}{2\Delta s} + b_1 \frac{(D_{21}T_x + D_{22}T_y)_u - (D_{21}T_x + D_{22}T_y)_d}{2\Delta n} + f.
\end{aligned}$$

For the diffusion tensor values we use the same weighted averaging procedure as before. The diffusion tensor values are taken both averaged and exact in the dual grid points. The products of the diffusion tensor components and the gradients can be combined. For instance, for  $\alpha_{ru}(D_{11}T_x)_r$  we have

$$\alpha_{ru}(D_{11}T_x)_{ru} = \alpha_{ru}(D_{11})_{ru} \frac{T_{i+1,j+1} + T_{i+1,j} - T_{i,j+1} - T_{i,j}}{2h}.$$

Note that due to symmetry we will end up with the original symmetric scheme for any set of coordinates  $(x_r, y_r), (x_l, y_l), (x_u, y_u), (x_d, y_d)$ . To create a unique scheme, we introduce a weighting factor  $\omega \in [0, 1]$  for

the perpendicular part of the divergence approximation. This will increase the conservation errors a bit but may improve the behavior near high gradients in  $n$ -direction. This weighted scheme is not consistent for  $D_{\perp} \neq 0$  if  $\omega \neq 1$ .

For the locations of the stencil we take a step  $\Delta s$  in the direction and counterdirection of the field line, and a step  $\Delta n$  perpendicular to the field line and construct a stencil using the local weights. The unit direction vector we use to align the stencil is obtained by normalized averaging of the unit direction vectors in the surrounding points  $(i \pm 1/2, j \pm 1/2), (i \pm 1/2, j \mp 1/2)$ .

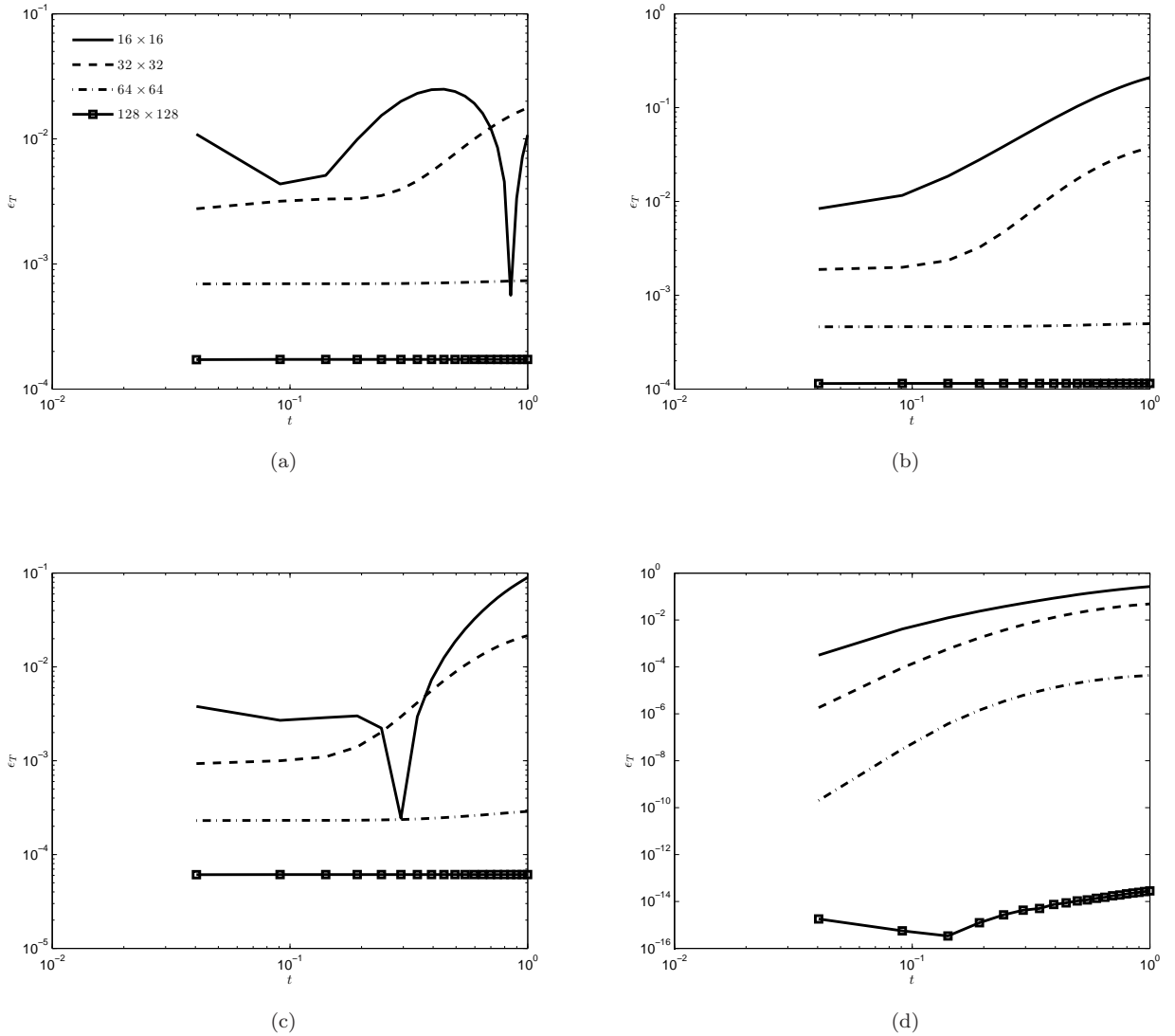


Figure 16:  $\epsilon_T$  error of the local symmetric scheme for a two-dimensional diffusion test case with a Gaussian initial distribution,  $D_{\perp} = 0, \sigma = 0.05, t_{end} = 1, d = 0.25, x, y \in [-2, 2]$  (a)  $\omega = 0.25$  (b)  $\omega = 0.5$  (c)  $\omega = 0.75$  (d)  $\omega = 1$

In figure16 we see that indeed the conservation of the total temperature is not maintained to machine accuracy, but it does converge with second order. Summarizing, the symmetric scheme by Günter et al.

has a gradient and divergence approximation that is aligned by construction. The local symmetric scheme introduced here was obtained by adding a weighting term to the perpendicular part of the divergence approximation. If the level of anisotropy is moderate the weighting term should be set to one for consistency.

## 6 Conclusion

We have developed and applied a new differencing method on a co-located grid that implements the concept of following the field line track within the stencil area to obtain the differencing points that are finally used in the approximation. In terms of accuracy and convergence the aligned methods are similar to exactly differentiating the interpolation schemes. The symmetric variants of our method are more accurate and less anisotropy-dependent than the standard asymmetric scheme by Günter et al. The symmetric scheme by Günter et al works well in maintaining the order of convergence for a wide variety of cases and it exhibits very low pollution of the perpendicular diffusion but it also seems to be more susceptible to number representation problems. This is apparent because the linear operator becomes ill-conditioned for large anisotropy ratios (noticeable above  $\varsigma = 10^9$ ).

We find that preserving continuity of the gradient is of key importance for maintaining the accuracy of the perpendicular diffusion. We see that in all cases where the aligned symmetric scheme and the symmetric interpolation scheme do not maintain order of convergence and/or the level of accuracy, the approximation of the perpendicular flux  $T_n$  determines this behavior. For all test cases the temperature gradient tangential to the field line is zero. For large gradients in magnetic field strength this term should also be considered. Over almost all the test cases, the symmetric scheme by Günter et al is better able to maintain the order of accuracy. The symmetric scheme by Günter et al does however show anisotropy-dependent accuracy for closed elliptic magnetic field line distributions, most likely due to a lack of symmetry in the solution. This anisotropy dependence is increased if we also make the diffusion-tensor components temperature dependent. This is caused by the interpolation required to get the temperature values in the flux points. For the tilted cases with temperature dependent diffusion coefficients our aligned and interpolated symmetric scheme show comparable and even superior results depending on the test case.

The non-conservative nature of the current scheme has an effect on the approximation of initial value problems with a non-aligned anisotropic diffusion tensor due to non-monotonous behavior in the direction perpendicular to the field line. As an improvement we suggest a local symmetric scheme which is derived from the symmetric scheme by Günter et al.

## Acknowledgments

This work, supported by NWO and the European Communities under the contract of the Association EURATOM/FOM, was carried out within the framework of the European Fusion Program. The views and opinions expressed herein do not necessarily reflect those of the European Commission.

## A Taylor expansions

For the **asymmetric scheme** described in section 3.1 the local truncation errors of the different terms  $(D_{11}T_x)_x$ ,  $(D_{22}T_y)_y$ ,  $(D_{21}T_y)_x$  and  $(D_{21}T_x)_y$  are found by writing out the Taylor expansions

$$\begin{aligned} (DT_x)_x &: T_x D_x + T_{xx} D + h^2 \left[ \frac{1}{24} T_x D_{xxx} + \frac{1}{8} T_{xx} D_{xx} + \frac{1}{6} T_{xxx} D_x + \frac{1}{24} T_{xxxx} D \right] + \mathcal{O}(h^4), \\ (DT_y)_x &: T_y D_x + T_{xy} D + h^2 \left[ \frac{1}{24} T_y D_{xxx} + \frac{1}{144} T_{yyy} D_x + \frac{1}{8} T_{xy} D_{xx} + \frac{1}{6} T_{xyyy} D \right. \\ &\quad \left. + \frac{1}{6} T_{xxxy} D + \frac{1}{4} T_{xxy} D_x \right] + \mathcal{O}(h^4), \end{aligned}$$

and similarly for  $(DT_y)_y$  and  $(DT_x)_y$  respectively. Likewise for the **symmetric scheme** found in section 3.2 the approximations are given by

$$\begin{aligned} (DT_x)_x &: T_x D_x + T_{xx} D + h^2 \left[ T_x \left( \frac{1}{8} D_{xyy} + \frac{1}{24} D_{xxx} \right) + T_{xx} \left( \frac{1}{8} D_{yy} + \frac{1}{8} D_{xx} \right) + \frac{1}{4} T_{xy} D_{xy} \right. \\ &\quad \left. + \frac{1}{4} T_{xyy} D_x + \frac{1}{4} T_{yyx} D_y + \frac{1}{6} T_{xxx} D_x + \frac{1}{4} T_{xxyy} D + \frac{1}{12} T_{xxxx} D \right] + \mathcal{O}(h^4), \\ (DT_y)_x &: T_y D_x + T_{xy} D + h^2 \left[ T_y \left( \frac{1}{8} D_{xyy} + \frac{1}{24} D_{xxx} \right) + T_{xy} \left( \frac{1}{8} D_{yy} + \frac{1}{8} D_{xx} \right) + \frac{1}{4} T_{yy} D_{xy} \right. \\ &\quad \left. + \frac{1}{24} T_{yyy} D_x + \frac{1}{16} T_{xyy} D_y + \frac{1}{16} T_{yxx} D_x + \frac{1}{6} T_{xyyy} D + \frac{1}{6} T_{yxxx} D \right] + \mathcal{O}(h^4), \end{aligned}$$

and similarly for  $(DT_y)_y$  and  $(DT_x)_y$  respectively. Similar to section 3.4.2, the approximations for the **aligned finite-difference scheme** are given by

$$\begin{aligned} \mathcal{A}_1 &= (D_{\parallel} - D_{\perp}) (c_8 b_1 - c_7 b_2) \left( b_1^2 c_7^{b_2} - b_2^2 c_8^{b_1} - b_1 b_2 c_7^{b_1} + b_1 b_2 c_8^{b_2} \right) \\ &\quad + h_*^2 (D_{\parallel} - D_{\perp}) \left[ (-c_3 b_1^2 b_2 + c_2 b_1 b_2^2) \left( b_1^2 c_7^{b_2} - b_2^2 c_8^{b_1} - b_1 b_2 c_7^{b_1} + b_1 b_2 c_8^{b_2} \right) \right. \\ &\quad \left. + (c_8 b_1 - c_7 b_2) \left( -b_1^2 b_2^2 c_2^{b_1} + b_1^2 b_2^2 c_3^{b_2} + b_1^3 b_2 c_2^{b_2} - b_1 b_2^3 c_3^{b_1} \right) \right] + \mathcal{O}(h_*^4), \\ \mathcal{A}_2 &= (D_{\parallel} - D_{\perp}) (c_7 b_1 + c_8 b_2) \left( b_2^2 c_7^{b_1} + b_1^2 c_8^{b_2} - b_1 b_2 c_7^{b_2} - b_1 b_2 c_8^{b_1} \right) \\ &\quad + h_*^2 (D_{\parallel} - D_{\perp}) \left[ (c_2 b_1^2 b_2 + c_3 b_1 b_2^2) \left( b_2^2 c_7^{b_1} + b_1^2 c_8^{b_2} - b_1 b_2 c_7^{b_2} - b_1 b_2 c_8^{b_1} \right) \right. \\ &\quad \left. + (c_7 b_1 + c_8 b_2) \left( b_1^2 b_2^2 c_2^{b_2} + b_1^2 b_2^2 c_3^{b_1} - b_1 b_2^3 c_2^{b_1} - b_1^3 b_2 c_3^{b_2} \right) \right] + \mathcal{O}(h_*^4), \\ \mathcal{A}_3 &= 2D_{\parallel} (b_1^2 c_4 + b_2^2 c_5 + b_1 b_2 c_6) + 2D_{\perp} (b_2^2 c_4 + b_1^2 c_5 - b_1 b_2 c_6) + h_*^2 (2D_{\parallel} + 2D_{\perp}) b_1^2 b_2^2 c_1 + \mathcal{O}(h_*^4), \\ \mathcal{A}_4 &= (c_7 b_1 + c_8 b_2) \left( c_7^{D_{\parallel}} b_1 + c_8^{D_{\parallel}} b_2 \right) + (-c_7 b_2 + c_8 b_1) \left( -c_7^{D_{\perp}} b_2 + c_8^{D_{\perp}} b_1 \right) \\ &\quad + h_*^2 \left[ b_1^3 b_2 \left( c_2 c_7^{D_{\parallel}} + c_7 c_2^{D_{\parallel}} \right) + b_2^3 b_1 \left( c_3 c_8^{D_{\parallel}} + c_8 c_3^{D_{\parallel}} \right) + b_1^2 b_2^2 \left( c_2 c_8^{D_{\parallel}} + c_8 c_2^{D_{\parallel}} + c_3 c_7^{D_{\parallel}} + c_7 c_3^{D_{\parallel}} \right) \right] \\ &\quad + h_*^2 \left[ -b_1^3 b_2 \left( c_3 c_8^{D_{\perp}} + c_8 c_3^{D_{\perp}} \right) - b_2^3 b_1 \left( c_2 c_7^{D_{\perp}} + c_7 c_2^{D_{\perp}} \right) + b_1^2 b_2^2 \left( c_3 c_7^{D_{\perp}} + c_7 c_3^{D_{\perp}} + c_2 c_8^{D_{\perp}} + c_8 c_2^{D_{\perp}} \right) \right] + \mathcal{O}(h_*^4), \end{aligned}$$

where it should be noted that here  $h_* = \Delta s = \Delta n$  represents the step size in the aligned stencil. If  $h_*$  goes to zero we get

$$\begin{aligned}\mathcal{A}_1 &= (D_{\parallel} - D_{\perp})(c_8 b_1 - c_7 b_2) \left( b_1^2 c_7^{b_2} - b_2^2 c_8^{b_1} - b_1 b_2 c_7^{b_1} + b_1 b_2 c_8^{b_2} \right), \\ \mathcal{A}_2 &= (D_{\parallel} - D_{\perp})(c_7 b_1 + c_8 b_2) \left( b_2^2 c_7^{b_1} + b_1^2 c_8^{b_2} - b_1 b_2 c_7^{b_2} - b_1 b_2 c_8^{b_1} \right), \\ \mathcal{A}_3 &= 2D_{\parallel} (b_1^2 c_4 + b_2^2 c_5 + b_1 b_2 c_6) + 2D_{\perp} (b_2^2 c_4 + b_1^2 c_5 - b_1 b_2 c_6), \\ \mathcal{A}_4 &= (c_7 b_1 + c_8 b_2) \left( c_7^{D_{\parallel}} b_1 + c_8^{D_{\parallel}} b_2 \right) + (-c_7 b_2 + c_8 b_1) \left( -c_7^{D_{\perp}} b_2 + c_8^{D_{\perp}} b_1 \right),\end{aligned}$$

which is equal to the exact differentiation scheme from section 3.5.

## B Linear operator

For the determination of the linear operator it is convenient to collect the factors for each temperature value

$$T(x, y) = a_{i,j}T_{i,j} + a_{i+1,j}T_{i+1,j} + a_{i-1,j}T_{i-1,j} + a_{i,j+1}T_{i,j+1} + a_{i,j-1}T_{i,j-1} \\ + a_{i+1,j+1}T_{i+1,j+1} + a_{i-1,j+1}T_{i-1,j+1} + a_{i+1,j-1}T_{i+1,j-1} + a_{i-1,j-1}T_{i-1,j-1},$$

where for the Vandermonde coefficients we have

$$a_{i,j} = \frac{x^2 y^2}{h^4} - \frac{x^2}{h^2} - \frac{y^2}{h^2} + 1, \\ a_{i\pm 1,j} = \frac{1}{2} \left( -\frac{x^2 y^2}{h^4} \mp \frac{y^2 x}{h^3} + \frac{x^2}{h^2} \pm \frac{x}{h} \right), \\ a_{i,j\pm 1} = \frac{1}{2} \left( -\frac{x^2 y^2}{h^4} \mp \frac{x^2 y}{h^3} + \frac{y^2}{h^2} \pm \frac{y}{h} \right), \\ a_{i\pm 1,j+1} = \frac{1}{4} \left( \frac{x^2 y^2}{h^4} + \frac{x^2 y}{h^3} \pm \frac{y^2 x}{h^3} \pm \frac{xy}{h^2} \right), \\ a_{i\pm 1,j-1} = \frac{1}{4} \left( \frac{x^2 y^2}{h^4} - \frac{x^2 y}{h^3} \pm \frac{y^2 x}{h^3} \mp \frac{xy}{h^2} \right),$$
(15)

and for the symmetric coefficients

$$a_{i,j} = \frac{x^2 y^2}{h^4} - \frac{1}{2} \frac{x^2}{h^2} - \frac{1}{2} \frac{y^2}{h^2} + 1, \\ a_{i\pm 1,j} = \frac{1}{2} \left( -\frac{x^2 y^2}{h^4} \mp \frac{y^2 x}{h^3} + \frac{1}{2} \frac{x^2}{h^2} - \frac{1}{2} \frac{y^2}{h^2} \pm \frac{1}{2} \frac{x}{h} \right), \\ a_{i,j\pm 1} = \frac{1}{2} \left( -\frac{x^2 y^2}{h^4} \mp \frac{x^2 y}{h^3} - \frac{1}{2} \frac{x^2}{h^2} + \frac{1}{2} \frac{y^2}{h^2} \pm \frac{1}{2} \frac{y}{h} \right), \\ a_{i\pm 1,j+1} = \frac{1}{4} \left( \frac{x^2 y^2}{h^4} + \frac{x^2 y}{h^3} \pm \frac{y^2 x}{h^3} + \frac{1}{2} \frac{x^2}{h^2} + \frac{1}{2} \frac{y^2}{h^2} \pm \frac{xy}{h^2} \pm \frac{1}{2} \frac{x}{h} + \frac{1}{2} \frac{y}{h} \right), \\ a_{i\pm 1,j-1} = \frac{1}{4} \left( \frac{x^2 y^2}{h^4} - \frac{x^2 y}{h^3} \pm \frac{y^2 x}{h^3} + \frac{1}{2} \frac{x^2}{h^2} + \frac{1}{2} \frac{y^2}{h^2} \mp \frac{xy}{h^2} \pm \frac{1}{2} \frac{x}{h} - \frac{1}{2} \frac{y}{h} \right).$$
(16)

The terms in equation (3) can be approximated by the following schemes:

$$\mathcal{A}_1 = -(D_{\parallel} - D_{\perp})N \frac{T_u - T_d}{2\Delta n}, \\ \mathcal{A}_2 = (D_{\parallel} - D_{\perp})S \frac{T_r - T_l}{2\Delta s}, \\ \mathcal{A}_3 = D_{\parallel} \frac{T_r - 2T_c + T_l}{\Delta s^2} + D_{\perp} \frac{T_u - 2T_c + T_d}{\Delta n^2}, \\ \mathcal{A}_4 = \frac{D_{\parallel r} - D_{\parallel l}}{2\Delta s} \frac{T_r - T_l}{2\Delta s} + \frac{D_{\perp u} - D_{\perp d}}{2\Delta n} \frac{T_u - T_d}{2\Delta n}.$$

Using the previous expressions for  $a_{i,j}$ ,  $a_{i\pm 1,j}$ ,  $a_{i,j\pm 1}$ ,  $a_{i\pm 1,j-1}$  and  $a_{i\pm 1,j+1}$  the linear operator can be written as

$$\tilde{f}_{i,j} \approx T_{i,j} d_c + \sum_{n=-1}^1 \sum_{m=-1}^1 [a_{i+m,j+n}(x_r, y_r) d_r + a_{i+m,j+n}(x_l, y_l) d_l \\ + a_{i+m,j+n}(x_u, y_u) d_u + a_{i+m,j+n}(x_d, y_d) d_d] T_{i+m,j+n},$$

where  $\tilde{f}_{i,j}$  is the local source value, including boundary terms. The terms  $d_{l,r,u,d,c}$  are described by

$$\begin{aligned} d_r &= (D_{\parallel} - D_{\perp}) \frac{S}{2\Delta s} + \frac{D_{\parallel}}{\Delta s^2} + \frac{D_{\parallel r} - D_{\parallel l}}{4\Delta s^2}, \\ d_l &= -(D_{\parallel} - D_{\perp}) \frac{S}{2\Delta s} + \frac{D_{\parallel}}{\Delta s^2} - \frac{D_{\parallel r} - D_{\parallel l}}{4\Delta s^2}, \\ d_u &= -(D_{\parallel} - D_{\perp}) \frac{N}{2\Delta n} + \frac{D_{\perp}}{\Delta n^2} + \frac{D_{\perp u} - D_{\perp d}}{4\Delta n^2}, \\ d_d &= (D_{\parallel} - D_{\perp}) \frac{N}{2\Delta n} + \frac{D_{\perp}}{\Delta n^2} - \frac{D_{\perp u} - D_{\perp d}}{4\Delta n^2}, \\ d_c &= -2 \frac{D_{\parallel}}{\Delta s^2} - 2 \frac{D_{\perp}}{\Delta n^2}. \end{aligned}$$

For the local symmetric coefficients we consider the derivatives

$$\begin{aligned} T_x(x, y) &= a_{i,j} T_{i,j} + a_{i+1,j} T_{i+1,j} + a_{i-1,j} T_{i-1,j} + a_{i,j+1} T_{i,j+1} + a_{i,j-1} T_{i,j-1} \\ &\quad + a_{i+1,j+1} T_{i+1,j+1} + a_{i-1,j+1} T_{i-1,j+1} + a_{i+1,j-1} T_{i+1,j-1} + a_{i-1,j-1} T_{i-1,j-1}, \\ T_y(x, y) &= b_{i,j} T_{i,j} + b_{i+1,j} T_{i+1,j} + b_{i-1,j} T_{i-1,j} + b_{i,j+1} T_{i,j+1} + b_{i,j-1} T_{i,j-1} \\ &\quad + b_{i+1,j+1} T_{i+1,j+1} + b_{i-1,j+1} T_{i-1,j+1} + b_{i+1,j-1} T_{i+1,j-1} + b_{i-1,j-1} T_{i-1,j-1}, \end{aligned}$$

where

$$\begin{aligned} a_{i,j} &= \frac{1}{2h} (-\alpha_{ru} + \alpha_{lu} + \alpha_{ld} - \alpha_{rd}), & b_{i,j} &= \frac{1}{2h} (-\alpha_{ru} - \alpha_{lu} + \alpha_{ld} + \alpha_{rd}), \\ a_{i+1,j} &= \frac{1}{2h} (\alpha_{ru} + \alpha_{rd}), & b_{i+1,j} &= \frac{1}{2h} (-\alpha_{ru} + \alpha_{rd}), \\ a_{i-1,j} &= \frac{1}{2h} (-\alpha_{lu} - \alpha_{ld}), & b_{i-1,j} &= \frac{1}{2h} (-\alpha_{lu} + \alpha_{ld}), \\ a_{i,j+1} &= \frac{1}{2h} (-\alpha_{ru} + \alpha_{lu}), & b_{i,j+1} &= \frac{1}{2h} (\alpha_{ru} + \alpha_{lu}), \\ a_{i,j-1} &= \frac{1}{2h} (\alpha_{ld} - \alpha_{rd}), & b_{i,j-1} &= \frac{1}{2h} (-\alpha_{ld} - \alpha_{rd}), \\ a_{i+1,j+1} &= \frac{\alpha_{ru}}{2h}, & b_{i+1,j+1} &= \frac{\alpha_{ru}}{2h}, & a_{i-1,j-1} &= -\frac{\alpha_{ld}}{2h}, & b_{i-1,j-1} &= -\frac{\alpha_{ld}}{2h}, \\ a_{i-1,j+1} &= -\frac{\alpha_{lu}}{2h}, & b_{i-1,j+1} &= \frac{\alpha_{lu}}{2h}, & a_{i+1,j-1} &= \frac{\alpha_{rd}}{2h}, & b_{i+1,j-1} &= -\frac{\alpha_{rd}}{2h}, \end{aligned}$$

where the  $\alpha$ 's are defined in section 5.2.

## References

- [1] Discrete Exterior Calculus.
- [2] I. Aavatsmark. Multipoint flux approximation methods for quadrilateral grids. *9<sup>th</sup> International Forum on Reservoir Simulation*, 2007.
- [3] I. Aavatsmark, T. Barkve, Ø. Bøe, and T. Mannseth. Discretization on non-orthogonal, curvilinear grids for multi-phase flow. *Proc. of the 4th European Conf. on the Mathematics of Oil Recovery, Røros*, 6, 1994.
- [4] I. Aavatsmark, T. Barkve, Ø. Bøe, and T. Mannseth. Discretization on non-orthogonal, quadrilateral grids for inhomogeneous, anisotropic media. *J. Comput. Phys.*, 127:2–14, 1996.

- [5] I. Aavatsmark, T. Barkve, Ø. Bøe, and T. Mannseth. Discretization on unstructured grids for inhomogeneous, anisotropic media. part i: derivation of the methods. *SIAM J. Sci. Comp.*, 19(5):1700–1716, 1998.
- [6] I. Aavatsmark, T. Barkve, Ø. Bøe, and T. Mannseth. Discretization on unstructured grids for inhomogeneous, anisotropic media. part ii: discussion and numerical results. *SIAM J. Sci. Comput.*, 19(5):1717–1736, 1998.
- [7] L. Agélas, A. Di Pietro, and J. Droniou. The g method for heterogeneous anisotropic diffusion on general meshes. *Math. Mod. Num. Anal.*, 4(44):597–625, 2010.
- [8] C. Aricò and T. Tucciarelli. Monotonic solution of heterogeneous anisotropic diffusion problems. *J. Comput. Phys.*, 252:219–249, 2013.
- [9] I. Babuška and M. Suri. On locking and robustness in the finite element method. *SIAM J. Num. Anal.*, 220:751–771, 1992.
- [10] F. Bassi and S. Rebay. A high-order accurate discontinuous finite element method for the numerical solution of the compressible Navier-Stokes equations. *J. Comput. Phys.*, 131(2):267–279, 1997.
- [11] J. Bonelle and A. Ern. Analysis of compatible discrete operator schemes for elliptic problems on polyhedral meshes. *ESAIM: Mathematical Modelling and Numerical Analysis*, 48(2):553–581, 2014.
- [12] J. Breil and P.-H. Maire. A cell-centered diffusion scheme on two-dimensional unstructured meshes. *J. Comput. Phys.*, 224:785–823, 2007.
- [13] F. Brezzi, K. Lipnikov, and M. Shashkov. Convergence of the mimetic finite difference method for diffusion problems on polyhedral meshes. *SIAM J. Num. Anal.*, 43(5):1872–1896, 2005.
- [14] F. Brezzi, K. Lipnikov, and V. Simoncini. A family of mimetic finite difference methods on polygonal and polyhedral meshes. *Math. Mod. Meth. Appl. Sci.*, 15:1533–1551, 2005.
- [15] B. Cockburn and C.-W. Shu. The local discontinuous Galerkin method for time-dependent convection-diffusion systems. *SIAM J. Numer. Anal.*, 35:2440–2463, 1998.
- [16] P. Degond, F. Deluzet, A. Lozinski, J. Narski, and C. Negulescu. Duality-based Asymptotic-Preserving method for highly anisotropic diffusion equations. *ArXiv e-prints*, August 2010.
- [17] P. Degond, F. Deluzet, and C. Negulescu. An asymptotic preserving scheme for strongly anisotropic elliptic problems. *Multiscale Model. Simul.*, 8(2), 2009.
- [18] P. Degond, A. Lozinski, J. Narski, and C. Negulescu. An Asymptotic-Preserving method for highly anisotropic elliptic equations based on a micro-macro decomposition. *J. Comput. Phys.*, 231(7):2724–2740, 2012.
- [19] D. del Castillo-Negrete and L. Chacón. Local and nonlocal parallel heat transport in general magnetic fields. *Phys. Rev. Lett.*, 106(19), 2011.
- [20] D. del Castillo-Negrete and L. Chacón. Parallel heat transport in integrable and chaotic magnetic fields. *Phys. Plasmas*, 19(5):1–5, 2012.
- [21] J. Douglas Jr. and T. Dupont. Interior penalty procedures for elliptic and parabolic Galerkin methods. In *Computing Methods in Applied Sciences*, volume 58 of *Lecture Notes in Phys.*, page 207–216. 1976.
- [22] J. Droniou. Finite volume schemes for diffusion equations: introduction to and review of modern methods. *HAL report*, (hal-00813613), 2013.

- [23] J. Droniou and R. Eymard. A mixed finite volume scheme for anisotropic diffusion problems on any grid. *Numer. Math.*, 105(1):35–71, 2006.
- [24] J. Droniou, R. Eymard, T. Gallouët, and R. Herbin. A unified approach to mimetic finite difference, hybrid finite volume and mixed finite volume methods. *Math. Mod. Meth. Appl. Sci.*, 20(2):265–295, 2008.
- [25] M.G. Edwards and C.F. Rogers. Finite volume discretization with imposed flux continuity for the general tensor pressure equation. *Comp. Geosci.*, 2:259–290, 1998.
- [26] R. Eymard, T. Gallouët, and R. Herbin. A cell-centred finite-volume approximation for anisotropic diffusion operators on unstructured meshes in any space dimension. *IMA J. Numer. Anal.*, 26:326–353, 2006.
- [27] R. Eymard, T. Gallouët, and R. Herbin. Discretization of heterogeneous and anisotropic diffusion problems on general nonconforming meshes, SUSHI: a scheme using stabilization and hybrid interfaces. *IMA J. Numer. Anal.*, 30(4):1009–1043, 2010.
- [28] R. Eymard, G. Henry, R. Herbin, F. Hubert, R. Klöforn, and G. Manzini. *Finite Volumes for Complex Applications VI, Problems and Perspectives*, volume 4 of *Springer Proceeding in Mathematics*, chapter 3D Benchmark on discretization schemes for anisotropic diffusion problems on general grids, pages 895–930. ISTE, 2011.
- [29] G. Gassner, F. Lörcher, and C.-D. Munz. A contribution to the construction of diffusion fluxes for finite volume and discontinuous Galerkin schemes. *J. Comput. Phys.*, 224(2):1049–1063, 2007.
- [30] S. Günter, K. Lackner, and C. Tichmann. Finite element and higher order difference formulations for modelling heat transport in magnetised plasmas. *J. Comput. Phys.*, 226:2306–2316, 2007.
- [31] S. Günter, Q. Yu, J. Krüger, and K. Lackner. Modelling of heat transport in magnetised plasmas using non-aligned coordinates. *J. Comput. Phys.*, 209:354–370, 2005.
- [32] R. Herbin and F. Hubert. *Finite Volumes for Complex Applications V*, chapter Benchmark on discretization schemes for anisotropic diffusion problems on general grids, pages 659–692. ISTE, 2008.
- [33] F. Hermeline. A finite volume method for the approximation of diffusion operators on distorted meshes. *J. Comput. Phys.*, (160):481–499, 2000.
- [34] F. Hermeline. A finite volume method for approximating 3d diffusion operators on general meshes. *J. Comput. Phys.*, (228):5763–5786, 2009.
- [35] A.N. Hirani. *Discrete Exterior Calculus*. PhD thesis, California Institute of Technology, 2003.
- [36] A.N. Hirani, K.B. Nakshatrala, and J.H. Chaudhry. Numerical method for Darcy flow derived using Discrete Exterior Calculus. *ArXiv e-prints*, 2008.
- [37] M. Hözl. *Diffusive Heat Transport across Magnetic Islands and Stochastic Layers in Tokamaks*. PhD thesis, Technische Universität München, Max-Planck-Institut für Plasmaphysik, 2010.
- [38] J. Hyman, J. Morel, M. Shashkov, and S. Steinberg. Mimetic finite difference methods for diffusion equations. *Comp. Geosci.*, 6:333–352, 2002.
- [39] J. Hyman, M. Shashkov, and S. Steinberg. The numerical solution of diffusion problems in strongly heterogeneous non-isotropic materials. *J. Comput. Phys.*, 132:130–148, 1997.
- [40] P. Jacq, P.H. Maire, and R. Abgrall. A high-order cell-centered finite volume scheme for simulating three dimensional anisotropic diffusion equations on unstructured grids. *HAL report*, (hal-00835537), 2013.

- [41] R.A. Klausen and T.F. Russell. Relationships among some locally conservative discretization methods which handle discontinuous coefficients. *Comp. Geosci.*, 8:341–377, 2004.
- [42] J. Kreeft, A. Palha, and M. Gerritsma. Mimetic framework on curvilinear quadrilaterals of arbitrary order. *ArXiv e-prints*, 2011.
- [43] C. Le Potier. A finite volume method for the approximation of highly anisotropic diffusion operators on unstructured meshes. *Finite Volumes for Complex Applications IV*, 2005.
- [44] C. Le Potier. Schéma volumes finis monotone pour des opérateurs de diffusion fortement anisotropes sur des maillages de triangles nonstructurés. *Comptes Rendus Mathématique*, 341(12):787–792, 2005.
- [45] C. Le Potier and T.H. Ong. A cell-centered scheme for heterogeneous anisotropic diffusion problems on general meshes. *Int. J. Fin. Vol.*, 8:1–40, 2012.
- [46] X. Li and W. Huang. An anisotropic mesh adaptation method for the finite element solution of heterogeneous anisotropic diffusion problems. *J. Comput. Phys.*, 229:8072–8094, 2010.
- [47] K. Lipnikov, G. Manzini, and D. Svyatskiy. Analysis of the monotonicity conditions in the mimetic finite difference method for elliptic problems. *J. Comput. Phys.*, 230:2620–2642, 2011.
- [48] K. Lipnikov and M. Shashkov. Local flux mimetic finite difference methods. *Numerische Mathematik*, 112:115–152, 2009.
- [49] K. Lipnikov, M. Shashkov, D. Svyatskiy, and Y. Vassilevski. Monotone finite volume schemes for diffusion equations on unstructured triangular and shape-regular polygonal meshes. *J. Comput. Phys.*, 227:492–512, 2007.
- [50] K. Lipnikov, M. Shashkov, and I. Yotov. Local flux mimetic finite difference methods. Technical Report LA-UR-05-8364, Los Alamos National laboratory, 2005.
- [51] K. Lipnikov, D. Svyatskiy, and Y. Vassilevski. Interpolation-free monotone finite volume method for diffusion equations on polygonal meshes. *J. Comput. Phys.*, 228:703–716, 2009.
- [52] P.-H. Maire and J. Breil. A high-order finite volume cell-centered scheme for anisotropic diffusion on two-dimensional unstructured grids. *J. Comput. Phys.*, 224(2):785–823, 2011.
- [53] P.-H. Maire and J. Breil. A nominally second-order accurate finite volume cell-centered scheme for anisotropic diffusion on two-dimensional unstructured grids. *J. Comput. Phys.*, 231:2259–2299, 2012.
- [54] E.T. Meier, V.S. Lukin, and U. Shumlak. Spectral element spatial discretization error in solving highly anisotropic heat conduction equation. *Comp. Phys. Comm.*, 181:837–841, 2010.
- [55] A. Mentrelli and C. Negulescu. Asymptotic preserving scheme for highly anisotropic, nonlinear diffusion equations. *J. Comput. Phys.*, 231(24):8229–8245, 2012.
- [56] J.E. Morel, R.M. Roberts, and M. Shashkov. A local support-operators diffusion discretization scheme for quadrilateral  $r - z$  meshes. *J. Comput. Phys.*, (144):17–51, 1998.
- [57] J. Narski and M. Ottaviani. Asymptotic Preserving scheme for strongly anisotropic parabolic equations for arbitrary anisotropy direction. *ArXiv e-prints*, March 2013.
- [58] J.T. Oden, I. Babuška, and C.E. Baumann. A discontinuous hp finite element method for diffusion problems. *J. Comput. Phys.*, 146(2):491–519, 1998.
- [59] T.H. Ong. *Schémas volumes finis pour des opérateurs de diffusion anisotropes hétérogènes sur des maillages non-conformes*. PhD thesis, Université Paris-Est, 2012.

- [60] A.J. Pasdunkorale and I.W. Turner. A second order control-volume finite element least-squares strategy for simulating diffusion in strongly anisotropic media. *J. Comp. Math.*, 23(1):1–16, 2005.
- [61] J. Peraire and P.-O. Persson. The compact discontinuous Galerkin (CDG) method for elliptic problems. *SIAM J. Sci. Comput.*, 30(4):1806–1824, 2008.
- [62] P.P. Rebelo, A. Palha, and M. Gerritsma. Mixed mimetic spectral element method applied to Darcy’s problem. *ArXiv e-prints*, April 2013.
- [63] P. Sharma and G.W. Hammett. Preserving monotonicity in anisotropic diffusion. *J. Comput. Phys.*, 227:123–142, 2007.
- [64] M. Shashkov and S. Steinberg. Support-operator finite-difference algorithms for general elliptic problems. *J. Comput. Phys.*, 118:131–151, 1995.
- [65] C.R. Sovinec, A.H. Glasser, T.A. Gianakon, D.C. Barnes, R.A. Nebel, S.E. Kruger, D.D. Schnack, S.J. Plimpton, A. Tarditi, and M.S. Chu. Nonlinear magnetohydrodynamics simulation using high-order finite elements. *J. Comput. Phys.*, 195:355–386, 2004.
- [66] M.V. Umansky, M.S. Day, and T.D. Rognlien. On numerical solution of strongly anisotropic diffusion equation on misaligned grids. *Numerical Heat Transfer, Part B.*, 47:533–554, 2005.
- [67] B. Van Leer, M. Lo, and M. Van Raalte. A discontinuous Galerkin method for diffusion based on recovery. *AIAA-paper 4083*, 2007.
- [68] B. Van Leer and S. Nomura. Discontinuous Galerkin for diffusion. *AIAA-paper 5108*, 2005.